(Fig. 3a). There was slight irregularity of the end plate in the radiograph of the thoraco-lumbar spine (Fig. 3b). Based on the radiographic findings, this case was diagnosed as the Ribbing type (mild form) of MED with chondral lesions in bilateral knees.

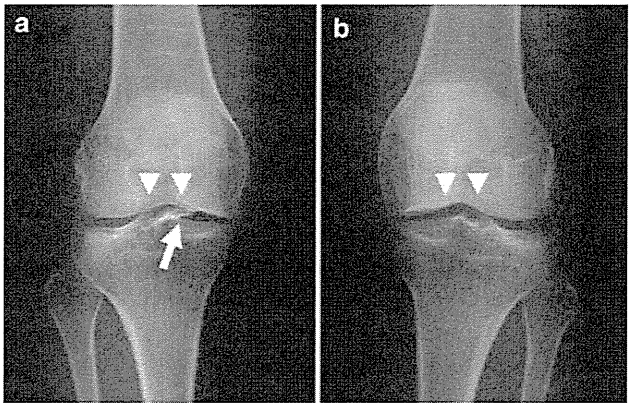

Fig. 1 Anteroposterior radiographs of both knees showed a shallow femoral trochlear groove (*arrowheads*) and flattening of the medial femoral condyle. **a** Radiograph of the right knee showing a loose body (*arrow*). **b** Radiograph of the left knee

Arthroscopy on both knees was performed. The articular cartilage of the bilateral MFC was detached from the subchondral bone. The cartilage defects extended down more than 50% of the cartilage depth but not through to the subchondral bone (Fig. 4). According to the International Cartilage Repair Society (ICRS) scoring system [10], the chondral lesions were Grade 3. There were 2 loose bodies (10 mm and 3 mm in diameter, respectively) in the right knee joint and these were excised.

Osteochondral autograft was performed for the left knee and for the right knee 22 months later, using the Osteochondral Autograft Transfer System (OATS^{TM}; Arthrex, Naples, FL, USA). Osteochondral autograft using this system involves obtaining small cylindrical osteochondral grafts from the minimum-weight-bearing periphery of the femoral condyles at the level of the patellofemoral joint and transplanting these to the recipient sites on the weight-bearing surfaces. Sizes of the lesions were 20 × 15 mm in the left MFC, and 20 × 10 mm in the right MFC. For the left knee, 6 osteochondral plugs 6 mm in diameter were harvested from the minimum-weight-bearing periphery of the ipsilateral patella-femoral joint and transplanted to the

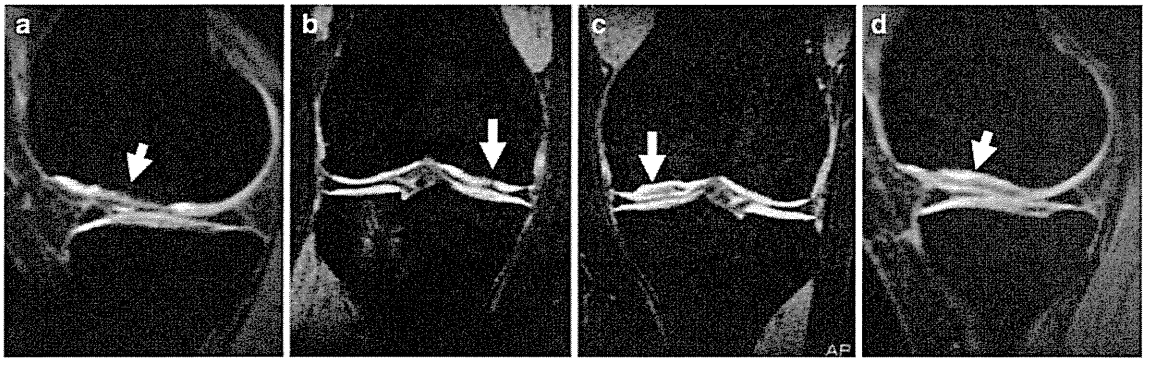

Fig. 2 T1-weighted magnetic resonance imaging (MRI) with fat suppression showed an irregular joint surface corresponding to the articular cartilage of the bilateral medial femoral condyle (*arrows*). **a** Coronal MRI of the right knee. **b** Sagittal image of the right knee. **c** Sagittal image of the left knee. **d** Coronal image of the left knee

Fig. 3 **a** Radiograph of the hip joints showed flattening of the femoral head and short neck. **b** There was slight irregularity of the end plate in the radiograph of the thoraco-lumbar spine

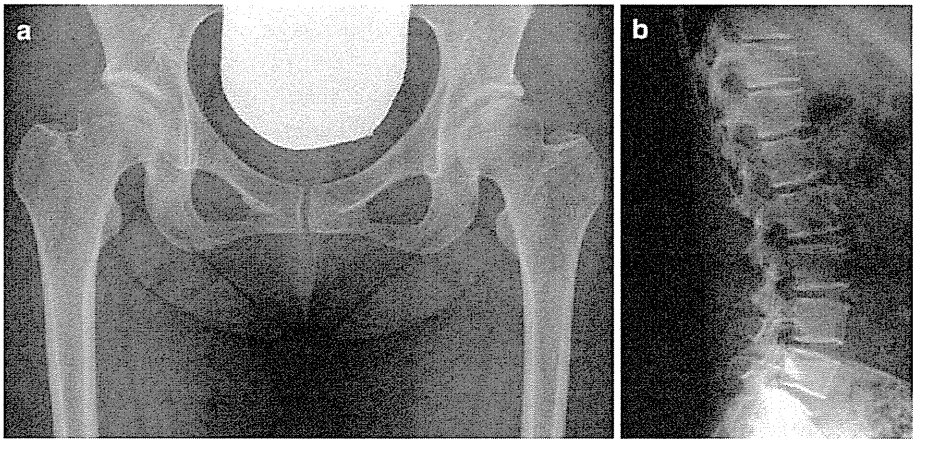

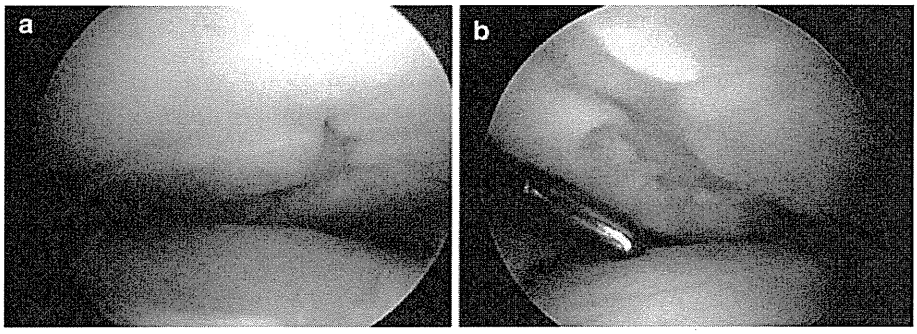

Fig. 4 Arthroscopy showed the chondral lesions of the medial femoral condyle of both knees. **a** Chondral lesion in the right knee. **b** Chondral lesion in the left knee

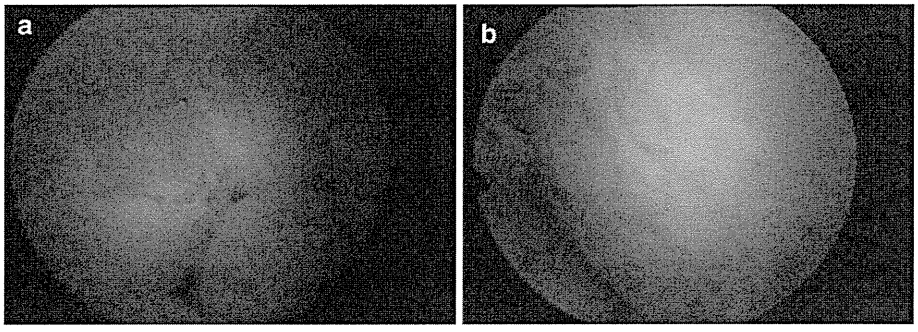

Fig. 5 **a** Intraoperative arthroscopic image of the recipient site of the right knee after osteochondral autograft. **b** Second-look arthroscopic image of the recipient site of the left knee 24 months after the surgery. The gaps surrounding the grafts were filled with fibrous cartilage-like tissue and the surface of the grafted area was totally smooth

chondral defect of the MFC. For the right knee, 4 osteochondral plugs 7 mm in diameter were transplanted to the chondral defect of the MFC (Fig. 5a). Bone plugs harvested from the host site were transplanted to the recipient site in exchange.

Postoperatively, passive range of motion exercise of the operated knee was allowed 3 days after the surgery, partial weight-bearing was allowed 2 weeks after the surgery, and full weight-bearing was allowed 12 weeks after the surgery.

Twenty-two months after the surgery, second-look arthroscopy was performed for the left knee at the same time as the osteochondral transplantation for the right knee. The gaps surrounding the grafts were filled with fibrous cartilage-like tissue and the surface of the grafted area was totally smooth. Palpation with a probe showed no instability of the grafts and the same elasticity as normal cartilage. According to ICRS cartilage repair assessment [10], the cartilage repair was graded as Grade I (12/12 points, normal) (Fig. 5b).

Ten years after the surgery on the left knee and 8 years after that on the right, the patient walked without limitation with no pain and had full range of motion in both knees. Radiographs at final follow up showed no apparent progression of osteoarthritis in either knee (Fig. 6). T1-weighted MRI with fat suppression 10 years after surgery of the right knee and 8 years after surgery of the left knee showed smooth cartilage surface and the same signal intensity of the grafted bone as the surrounding bone in the MFC (Fig. 7). VAS for activities of daily living was 90 mm for the right knee and 87 mm for the left knee.

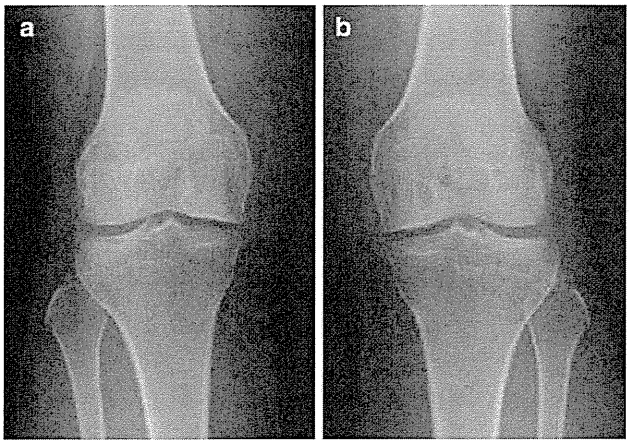

Fig. 6 Radiographs showed no apparent progression of osteoarthritis in the bilateral knee. The medial joint spaces were preserved. **a** Anteroposterior radiograph 8 years after surgery of the right knee. **b** Anteroposterior radiograph 10 years after surgery of the left knee

The patient was informed that data from the case would be submitted for publication, and gave her consent.

Discussion

MED is a form of osteochondrodysplasia characterized by abnormal epiphyseal growth with almost normal findings in the spine [1]. Classically, MED has been divided into the severe form (Fairbank type) [11] and the mild form (Ribbing type) [2]. Diagnostic criteria of MED are not

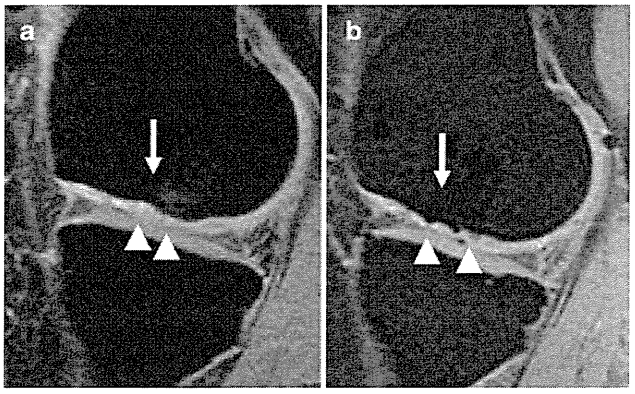

Fig. 7 T1-weighted MRI with fat suppression after the surgery showed a smooth cartilage surface (*arrowheads*) and the same signal intensity of the grafted bone as the surrounding bone in the medial femoral condyle (*arrows*). **a** Sagittal image of the right knee. **b** Sagittal image of the left knee

clear and diagnosis of MED for a patient after epiphyseal closure is often difficult. According to Eguchi, MED is diagnosed radiographically when there are abnormalities of the epiphysis in more than two joints with almost normal findings in the spine [12]. It was known that, although there are typical changes on the radiograph of the knee joint before epiphyseal closure, the changes are no longer discernible in the adult [13]. According to Miura et al. [4] after epiphyseal closure the most characteristic finding in the knee is a shallow femoral trochlear groove.

The radiographs of this patient showed a shallow femoral trochlear groove and slight osteoarthritis (subchondral sclerosis) in the knee despite her young age. They also showed flattening of the femoral heads and almost normal findings of the thoraco-lumbar spine with only slight irregularity of the end plate. The patient was therefore diagnosed with the Ribbing type (mild form) of MED. Although we did not have genetic evidence and obvious family history of the patient, it was possible to diagnose the patient with MED radiographically. Genetic screening is not indispensable to diagnosis of MED, because MED is not caused by a specific gene. According to Jakkula et al. [14] mutation analysis resulted in identification of 6 known genes in only 34% of patients and patients with MED had family history in only 40% of patients. Early osteoarthritis of the knee occurs in many patients of MED. It has been reported that gene mutations, for example of the cartilage oligomeric matrix protein (COMP) gene or matrilin3 (MATN3) can be the cause [15, 16]. Therefore, it is speculated that early osteoarthritic change or chondral lesions, for example OCD, occur because of abnormalities of the extracellular matrix.

Osteochondral autograft is one of the surgical procedures performed for patients with localized full-thickness cartilage defect in weight bearing synovial joints [6–9, 17], and has been used on OCD and traumatic cartilage defect. Hangody and Füles reported 10-year follow up results of autologous osteochondral grafting in the knee. According to them, results for 92% of patients after femoral condylar osteochondral transplantation were shown to be good to excellent [7]. There is concern about fragility of the extracellular matrix of the donor graft when performing osteochondral autografts in patients with MED. Thus, TKA and correction osteotomy have usually been performed for deformity and destruction of the knee [4, 5]. Our patient was young, her activity level was high, the alignment of the bilateral knees was almost normal, and the diagnosis was the mild form (Ribbing type) of MED. Although the cartilage defect was full-thickness in the weight-bearing area, the lesion was localized and no other degenerative lesion was observed inside the knee. Concomitant high tibial valgus osteotomy has been one option for reducing stress to the medial compartment and transplanted grafts. However, there was concern that the valgus alignment after the osteotomy might progress in future and, as a result, could have an adverse effect on the hip joints or ankle joints. No report was found of surgical treatment for early stage chondral lesion of the knee in a patient with MED, nor any report of osteochondral autograft for a chondral lesion with MED. Taking these risks and the lower invasiveness of the procedure into account, the osteochondral autograft alone was chosen for treatment of the chondral defects in this patient.

The long-term clinical and radiographical results of the patient were excellent, although an attentive and further long-term follow up is required because results of osteochondral autograft for a chondral lesion with MED have not previously been clear. In conclusion, osteochondral autograft can be one of the viable options for treating a regional chondral lesion of the knee even in a patient with MED. Careful preoperative assessment of the clinical features of the knee and the adjacent joints including hip and ankle joints is mandatory before performing this procedure.

Conflict of interest The authors declare that they have no conflict of interest in relation to the contents of this manuscript.

References

1. Haga N, Nakamura K, Takikawa K, Manabe N, Ikegawa S, Kimizuka M. Stature and severity in multiple epiphyseal dysplasia. J Pediatr Orthop. 1998;18:394–7.
2. Ribbing S. The hereditary multiple epiphyseal disturbance and its consequences for the aetiogenesis of local malacians. Particularly the osteochondrosis dissecans. Acta Orthop Scand. 1955;24:286–99.
3. Versteylen RJ, Zwemmer A, Lorié CAM, Schuur KH. Multiple epiphyseal dysplasia complicated by severe osteochondritis

dissecans of the knee. Incidence in two families. Skeletal Radiol. 1988;17:407–12.
4. Miura H, Noguchi Y, Matsuyasu H, Nagamine R, Urabe K, Matsuda S, Iwamoto Y. Clinical features of multiple epiphyseal dysplasia expressed in the knee. Clin Orthop Relat Res. 2000;380:184–90.
5. Sebik A, Sebik B, Kutluay E, Kuyurtar F, Ademoglu Y. The orthopaedic aspects of multiple epiphyseal dysplasia. Int Orthop. 1998;22:417–21.
6. Hangody L, Feczkó P, Bartha L, Bodó G, Kish G. Mosaicplasty for the treatment of articular defects of the knee and ankle. Clin Orthop Relat Res. 2001;391S:328–36.
7. Hangody L, Füles P. Autologous osteochondral mosaicplasty for treatment of full-thickness defects of weight-bearing joints: 10 years of experimental and clinical experience. J Bone Joint Surg Am. 2003;85A(suppl 2):25–32.
8. Hangody L, Ráthonyi GK, Duska Z, Vásárhelyi G, Füles P, Módis L. Autologous osteochondral mosaicplasty. Surgical technique. J Bone Joint Surg Am. 2004;86A(Suppl 1):65–72.
9. Jakob RP, Franz T, Gautier E, Mainil-Varlet P. Autologous osteochondral grafting in the knee: indication, results, and reflections. Clin Orthop Relat Res. 2002;401:170–84.
10. Brittberg M, Winalski CS. Evaluation of cartilage injuries and repair. J Bone Joint Surg Am. 2003;85A(suppl 2):58–69.
11. Fairbank T. Dysplasia epiphysialis multiplex. Br J Surg. 1947;34: 225–32.
12. Eguchi M Hip problems in multiple epiphyseal dysplasia. In: Itami Y, Nishino A editors. Constitutional Disease of Bone, Orthopaedic MOOK; 1982. p. 82–104 (in Japanese).
13. Unger S, Bonafé L, Superti-Furga A. Multiple epiphyseal dysplasia: clinical and radiographic features, differential diagnosis and molecular basis. Best Pract Res Clin Rheumatol. 2008;22: 19–32.
14. Jakkula E, Mäkitie O, Czarny-Ratacjzak M, Jackson GC, Damignani R, Susic M, Briggs MD, Cole WG, Ala-Kokko L. Mutations in the known genes are not the major cause of MED; distinctive phenotypic entities among patients with no identified mutations. Eur J Hum Genet. 2005;13:292–301.
15. Briggs MD, Hoffman SM, King LM, Olsen AS, Mohrenweiser H, Leroy JG, Mortier GR, Rimoin DL, Lachman RS, Gaines ES, Cekleniak JA, Knowlton RG, Cohn DH. Pseudochondroplasia and multiple epiphyseal dysplasia is due to mutations in the cartilage oligomeric matrix protein gene. Nat Genet. 1995;10: 330–6.
16. Chapman KL, Mortier GR, Chapman K, Loughlin J, Grant ME, Briggs MD. Mutations in the region encoding the von Willebrand factor A domain of matrilin-3 are associated with multiple epiphyseal dysplasia. Nat Genet. 2001;28:393–6.
17. Magnussen RA, Dunn WR, Carey JL, Spindler KP. Treatment of focal articular cartilage defects in the knee: a systematic review. Clin Orthop Relat Res. 2008;466:952–62.

Epigenetics 7:10, 1142–1150; October 2012; © 2012 Landes Bioscience

Paternal uniparental disomy 14 and related disorders

Placental gene expression analyses and histological examinations

Masayo Kagami,[1] Kentaro Matsuoka,[2] Toshiro Nagai,[3] Michiko Yamanaka,[4] Kenji Kurosawa,[5] Nobuhiro Suzumori,[6] Yoichi Sekita,[7] Mami Miyado,[1] Keiko Matsubara,[1] Tomoko Fuke,[1] Fumiko Kato,[1,8] Maki Fukami[1] and Tsutomu Ogata[1,8,*]

[1]Department of Molecular Endocrinology; National Research Institute for Child Health and Development; Tokyo, Japan; [2]Departments of Pathology; National Center for Child Health and Development; Tokyo, Japan; [3]Department of Pediatrics; Dokkyo University School of Medicine; Koshigaya, Japan; [4]Department of Integrated Women's Health; St. Luke's International Hospital; Tokyo, Japan; [5]Division of Medical Genetics; Kanagawa Children's Medical Center; Yokohama, Japan; [6]Department of Obstetrics and Gynecology; Nagoya City University Graduate School of Medicine; Nagoya, Japan; [7]Department of Pathology; Graduate School of Medicine; Osaka University, Osaka, Japan; [8]Department of Pediatrics; Hamamatsu University School of Medicine; Hamamatsu, Japan

Keywords: Upd(14)pat, microdeletion, placenta, expression dosage, histopathology, imprinting

Abbreviations: *PEGs*, paternally expressed genes; *MEGs*, maternally expressed genes; DMRs, differentially methylated regions; IG-DMR, *DLK1-MEG3* intergenic DMR; *RTL1as*, *RTL1* antisense; upd(14)pat, paternal uniparental disomy 14; BWS, Beckwith-Wiedemann syndrome; q-PCR, quantitative real-time PCR; CGH, oligoarray comparative genomic hybridization; LM, light microscopic; EM, electron microscopic; IHC, immunohistochemical

Although recent studies in patients with paternal uniparental disomy 14 [upd(14)pat] and other conditions affecting the chromosome 14q32.2 imprinted region have successfully identified underlying epigenetic factors involved in the development of upd(14)pat phenotype, several matters, including regulatory mechanism(s) for *RTL1* expression, imprinting status of *DIO3* and placental histological characteristics, remain to be elucidated. We therefore performed molecular studies using fresh placental samples from two patients with upd(14)pat. We observed that *RTL1* expression level was about five times higher in the placental samples of the two patients than in control placental samples, whereas *DIO3* expression level was similar between the placental samples of the two patients and the control placental samples. We next performed histological studies using the above fresh placental samples and formalin-fixed and paraffin-embedded placental samples obtained from a patient with a maternally derived microdeletion involving *DLK1*, the IG-DMR, the *MEG3*-DMR and *MEG3*. Terminal villi were associated with swollen vascular endothelial cells and hypertrophic pericytes, together with narrowed capillary lumens. DLK1, RTL1 and DIO3 proteins were specifically identified in vascular endothelial cells and pericytes, and the degree of protein staining was well correlated with the expression dosage of corresponding genes. These results suggest that *RTL1as*-encoded microRNA functions as a repressor of *RTL1* expression, and argue against *DIO3* being a paternally expressed gene. Furthermore, it is inferred that DLK1, DIO3 and, specially, RTL1 proteins, play a pivotal role in the development of vascular endothelial cells and pericytes.

Introduction

Human chromosome 14q32.2 region carries a cluster of imprinted genes including protein coding paternally expressed genes (*PEGs*) such as *DLK1* and *RTL1* (alias *PEG11*) and non-coding maternally expressed genes (*MEGs*) such as *MEG3* (alias *GTL2*) and *RTL1as* (*RTL1* antisense encoding microRNAs).[1,2] The 14q32.2 imprinted region also harbors two differentially methylated regions (DMRs), i.e., the germline-derived primary *DLK1-MEG3* intergenic DMR (IG-DMR) and the postfertilization-derived secondary *MEG3*-DMR.[1,2] Both DMRs are hypermethylated after paternal transmission and hypomethylated after maternal transmission in the body, whereas in the placenta the IG-DMR alone remains as a DMR and the *MEG3*-DMR is rather hypomethylated.[2] We have previously revealed that the hypomethylated IG-DMR and *MEG3*-DMR of maternal origin function as imprinting control centers in the placenta and the body, respectively, and that the IG-DMR functions hierarchically as an upstream regulator for the methylation pattern of the *MEG3*-DMR on the maternally inherited chromosome in the body, but not in the placenta.[3]

*Correspondence to: Tsutomu Ogata; Email: tomogata@hama-med.ac.jp
Submitted: 06/21/12; Revised: 08/20/12; Accepted: 08/22/12
http://dx.doi.org/10.4161/epi.21937

Consistent with these findings, paternal uniparental disomy 14 [upd(14)pat] results in a unique phenotype characterized by facial abnormality, small bell-shaped thorax with coat hanger appearance of the ribs, abdominal wall defects, placentomegaly and polyhydramnios.[2,4] We have studied multiple patients with upd(14)pat and related conditions, such as epimutations of the maternally derived DMRs and various types of microdeletions involving the maternally inherited imprinted region, suggesting that markedly increased *RTL1* expression is the major underlying factor for the development of upd(14)pat-like phenotype.[2] The notion of excessive *RTL1* expression is primarily based on the following mouse data indicating a trans-acting repressor function of *Rtl1as*-encoded microRNAs for *Rtl1* expression: (1) targeted deletion of the maternally derived IG-DMR causes maternal to paternal epigenotypic switch of the imprinted region, with ~4.5 times rather than ~2 times of *Rtl1* expression as well as ~2 times of *Dlk1* expression and nearly absent *Megs* expression, in the presence of two functional copies of *Pegs* and no functional copy of *Megs*[5] and; (2) targeted deletion of the maternally derived *Rtl1as* results in 2.5–3.0 times of *Rtl1* expression, in the presence of a single functional copy of *Rtl1*.[6] Similarly, in the human, typical upd(14)pat phenotype is observed in patients with epimutations that are likely associated with markedly increased *RTL1* expression because of the combination of two functional copies of *RTL1* and no functional copy of *RTL1as*, whereas relatively mild upd(14)pat-like phenotype is found in patients with maternally inherited microdeletions involving *RTL1as* that are likely accompanied by moderately elevated *RTL1* expression because of the combination of a single functional copy of *RTL1* and no functional copy of *RTL1as*.[2]

Human imprinting disorders are usually associated with placental abnormalities. For example, Beckwith-Wiedemann syndrome (BWS) and upd(14)pat are associated with placentomegaly,[4,7] and Silver-Russell syndrome is accompanied by hypoplastic placenta.[8] Similarly, mouse imprinting aberrations also usually affect placental growth and development.[9] In agreement with this, virtually all the imprinted genes studied to date are expressed in the placenta and play a pivotal role in the placental growth and development,[10] although placental structure is more or less different between placental animals.[11]

However, several matters remain to be clarified in upd(14)pat and related conditions. For example, it is unknown whether human *RTL1* expression is actually elevated in the absence of functional *RTL1as*-encoded microRNAs. It is also unknown whether *DIO3* is a *PEG*, although mouse *Dio3* has been shown to undergo partial imprinting.[12] In this regard, while we examined fresh blood cells, cultured skin fibroblasts and formalin-fixed and paraffin-embedded placental and body samples obtained from patients with upd(14)pat-like phenotype, precise assessment of *RTL1* and *DIO3* expression levels was impossible because of extremely low *RTL1* and *DIO3* expression levels in fresh blood cells and cultured skin fibroblasts and poor quality of RNAs extracted from paraffin-embedded tissues.[2,3] In addition, while cSNP genotyping has demonstrated paternal *DLK1* and *RTL1* expression and maternal *MEG3* expression in the body and the placenta,[2,3] no informative cSNP data showing paternal *DIO3* expression have been obtained.[2,3] Furthermore, although standard light microscopic (LM) examinations have been performed using formalin-fixed and paraffin-embedded placental samples, fine placental histopathological studies, such as electron microscopic (EM) examinations and immunohistochemical (IHC) examinations, remain to be performed.

To examine these unresolved matters, fresh placental tissues are highly useful, because precise quantitative real-time PCR (q-PCR) analyses and EM studies can be performed with fresh placentas. Thus, we performed q-PCR analyses and EM studies, as well as IHC studies with RTL1 antibodies produced by ourselves and commercially available DLK1 and DIO3 antibodies, using fresh placental samples obtained from two previously reported patients with prenatally diagnosed upd(14)pat.[13,14] We also performed IHC studies using formalin-fixed and paraffin-embedded placental samples obtained from a previously reported patient with a microdeletion involving *DLK1*, but not *RTL1* and *DIO3*,[2] to compare the placental protein expression levels between upd(14)pat and the microdeletion. Furthermore, we also studied a hitherto unreported patient with an unbalanced translocation involving the 14q32.2 imprinted region, to obtain additional data regarding the *RTL1-RTL1as* interaction and the primary factor for the development of upd(14)pat phenotype.

Results

Patients and samples. This study consisted of three previously reported patients with typical body and placental upd(14)pat phenotype and a normal karyotype (cases 1–3),[2,13-15] and a new patient with various non-specific features and a 46,XX,der(17)t(14;17)(q31;p13) karyotype accompanied by three copies of the distal 14q region and a single copy of the terminal 17p region (case 4) . Clinical phenotypes of cases 1–4 are summarized in **Table S1**. In brief, cases 1 and 2 were suspected to have upd(14)pat phenotype including bell-shaped thorax by prenatal ultrasound studies performed for polyhydroamnios, and were confirmed to have upd(14)pat by microsatellite analysis after birth. Case 3 was found to have typical upd(14)pat phenotype during infancy and was shown to have a maternally derived microdeletion affecting the chromosome 14q32.2 imprinted region. Case 4 had growth failure, developmental delay, multiple non-specific anomalies, and omphalocele. There was no history of polyhydramnios or placentomegaly. Thus, except for omphalocele, case 4 had no upd(14)pat-like phenotype. The parental karyotype was normal, indicating a de novo occurrence of the unbalanced translocation.

We obtained fresh placental samples immediately after birth from prenatally diagnosed cases 1 and 2 for molecular studies using genomic DNA and RNA, and fresh leukocyte samples from cases 1, 2 and 4 and their parents for molecular studies using genomic DNA. The fresh placental samples of cases 1 and 2 were also utilized for histopathological examinations, together with formalin-fixed and paraffin-embedded placental samples of case 3. For controls, we obtained three fresh placentas at 37 weeks of gestation, and fresh leukocytes from three adult subjects; for molecular studies using placentas, we prepared pooled samples

consisting of an equal amount of DNA or RNA extracted from each placenta.

Molecular studies in cases 1 and 2. We performed microsatellite analysis for 19 loci on chromosome 14 and bisulfite sequencing for the IG-DMR (CG4 and CG6) and the *MEG3*-DMR (CG7), using placental and leukocyte genomic DNA samples; while microsatellite analysis had been performed for 15 loci in case 1 and 16 loci in case 2, only leukocyte genomic DNA samples were examined in the previous study.[15] Consequently, we identified two peaks for *D14S609* and single peaks for the remaining loci in case 1 (the combination of paternal heterodisomy and isodisomy), and single peaks for all the examined loci in case 2 (apparently full paternal isodisomy) (**Table S2**). Furthermore, no trace of maternally inherited peak was identified in both placental and leukocyte genomic DNA samples (**Fig. 1**). Bisulfite sequencing showed that both the IG-DMR and the *MEG3*-DMR were markedly hypermethylated in the leukocytes of cases 1 and 2, whereas in the placental samples the IG-DMR was obviously hypermethylated and the *MEG3*-DMR was grossly hypomethylated to an extent similar to that identified in control placentas (**Fig. 2**). Furthermore, q-PCR analysis for placental RNA samples revealed that *DLK1*, *RTL1*, and *DIO3* expression levels were 3.3 times, 6.1 times and 1.9 times higher in the placental samples of case 1 than in the control placental samples, respectively, and were 3.1 times, 9.4 times and 1.7 times higher in the placental samples of case 2 than in the control placental samples, respectively (**Fig. 3A**). By contrast, the expressions of all *MEGs* examined were virtually absent in the placental samples of cases 1 and 2. PCR products were sufficiently obtained after 30 cycles for the fresh placental as well as leukocyte samples, consistent with high quality of DNA and RNA obtained from fresh materials.

Molecular studies in case 3. Detailed molecular findings have already been reported previously.[2] In brief, microsatellite analysis revealed biparentally derived homologs of chromosome 14, and a deletion analysis demonstrated a maternally inherited 108,768 bp microdeletion involving *DLK1*, the IG-DMR, the *MEG3*-DMR, and *MEG3*, but not affecting *RTL1*/*RTL1as*. Since loss of the DMRs causes maternal to paternal epigenotypic alteration,[2] it is predicted that case 3 has a single functional copy of *DLK1* and two functional copies of *RTL1* and *DIO3*, as well as no functional copy of *RTL1as* and other *MEGs*. Bisulfite sequencing showed that both the IG-DMR and the *MEG3*-DMR were markedly hypermethylated in leukocytes, whereas in the formalin-fixed and paraffin-embedded placental samples the IG-DMR was obviously hypermethylated and the *MEG3*-DMR was comprised of roughly two-thirds of hypermethylated clones and roughly one-third of hypomethylated clones. In addition, RT-PCR analysis for such placental samples indicated positive *PEGs* (especially *RTL1*) expression and absent *MEGs* expression. For the formalin-fixed and paraffin-embedded placental samples, PCR products could be obtained only after 35 cycles, because of poor quality (severe degradation) of DNA and RNA.

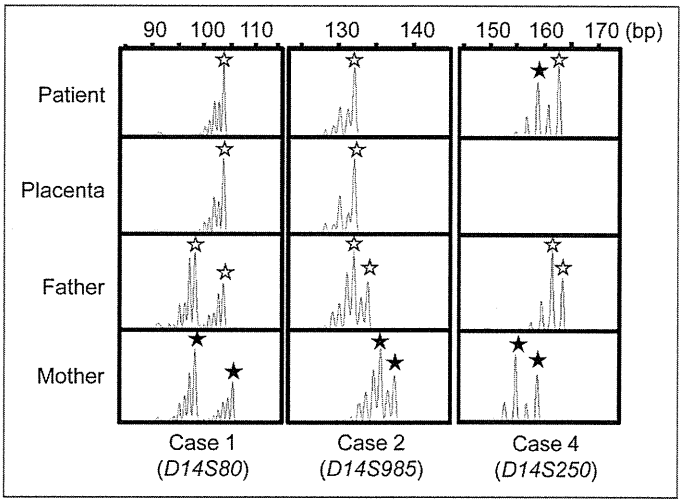

Figure 1. Representative results of microsatellite analysis, using leukocyte genomic DNA samples of the patient and the parents and placental genomic DNA samples. In cases 1 and 2, one of the two paternal peaks is inherited by the patients and the placentas, and no trace of maternal peaks is identified. In case 4, both paternally and maternally derived peaks are found in the patient, with the paternally derived long peak being larger than the maternally inherited short peak.

Molecular findings in case 4. We examined the presence or absence of the 14q32.2 imprinted region on the der(17) chromosome (**Fig. 4**). Oligoarray comparative genomic hybridization (CGH) indicated three copies of a ~19.6 Mb 14q31–qter region, and FISH analysis for four segments around the chromosome 14q32.2 imprinted region delineated positive signals on the der(17) chromosome as well as on the normal chromosome 14 homologs. This demonstrated the presence of the 14q32.2 imprinted region on the der(17) chromosome. In addition, similar oligoarray CGH and FISH analysis revealed loss of a ~455 kb region from the distal chromosome 17p (**Fig. S1**).

Thus, we investigated the parental origin of the translocated 14q distal region. Microsatellite analysis for *D14S250* and *D14S1007* on the translocated 14q distal region delineated biparentally derived two peaks, with paternally derived long PCR products showing larger peaks than maternally derived short PCR products (**Fig. 1**; **Table S2**). Since short products are usually more easily amplified than long products, this indicated paternal

Figure 2 (See opposite page). Bisulfite sequencing analysis of the IG-DMR (CG4 and CG6) and the *MEG3*-DMR (CG7), using leukocyte and placental genomic DNA samples. Filled and open circles indicate methylated and unmethylated cytosines at the CpG dinucleotides, respectively. Upper part: structure of CG4, CG6, and CG7. Pat, paternally derived chromosome; Mat, maternally derived chromosome. The PCR products for CG4 (311 bp) harbor 6 CpG dinucleotides and a G/A SNP (*rs12437020*), those for CG6 (428 bp) carry 19 CpG dinucleotides and a C/T SNP (*rs10133627*) and those for CG7 (168 bp) harbor 7 CpG dinucleotides. Lower part: the results of cases 1, 2, 4 and a control subject. Each horizontal line indicates a single subcloned allele. The control data represent the methylation patterns obtained with a leukocyte genomic DNA sample extracted from a single subject heterozygous for the G/A SNP (*rs12437020*) (body) and those obtained with a pooled DNA sample consisting of an equal amount of genomic DNA extracted from three control placentas homozygous for that SNP.

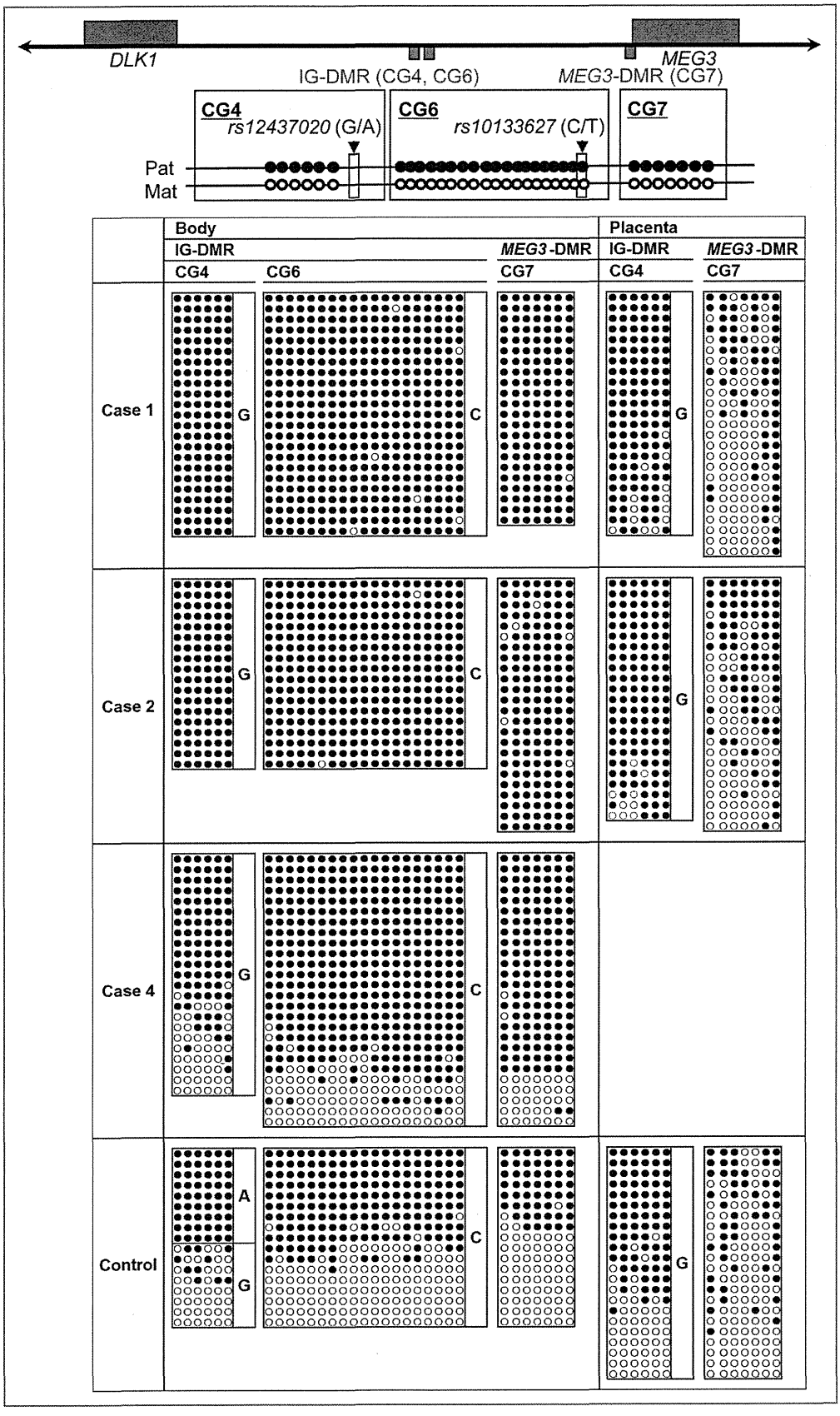

Figure 2. For figure legend, see page 1144.

origin of the der(17) chromosome harboring the chromosome14q32.2 imprinted region. Consistent with this, bisulfite sequencing showed moderate hypermethylation of the IG-DMR and the *MEG3*-DMR (Fig. 2).

Placental histopathological studies. We performed LM and EM studies, and IHC examinations (Fig. 5). LM examinations showed proliferated chorionic villi in cases 1–3. Capillary lumens were irregularly dilated with thickened endothelium in the stem to intermediate villi, but not in the terminal villi. Immature villi were present in case 3, probably because of 30 weeks of gestational age. Chorangioma was also identified in case 3. There was no villous chorangiosis, edematous change of villous stroma, or mesenchymal dysplasia characterized by grapelike vesicles in cases 1–3. Although the terminal villi exhibited no definitive abnormalities in the LM studies, EM examinations revealed swelling of vascular endothelial cells and hypertrophic change of pericytes in the terminal villi, together with narrowed capillary lumens, in cases 1 and 2.

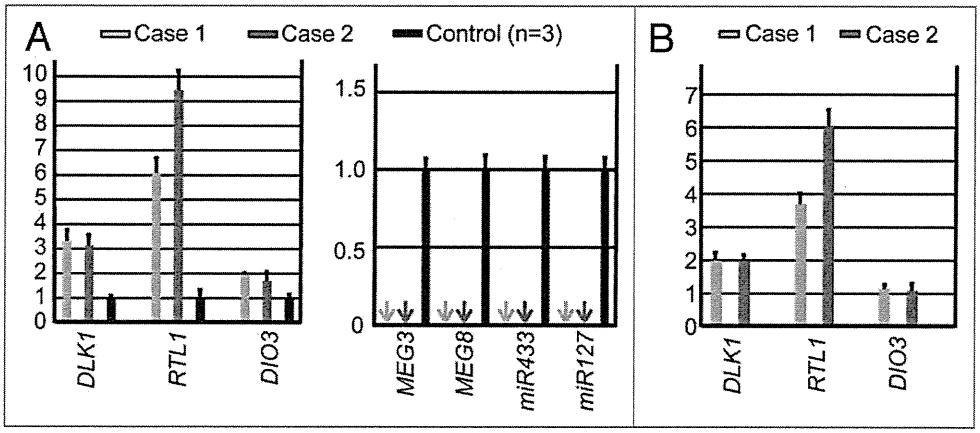

Figure 3. Quantitative real-time PCR analysis using placental samples. For a control, a pooled RNA sample consisting of an equal amount of total RNA extracted from three fresh control placentas was utilized. (A) Relative mRNA expression levels for *DLK1*, *RTL1*, and *DIO3* against *GAPDH* (mean ± SE) and lack of *MEGs* expression (indicated by arrows) (*miR433* and *miR127* are encoded by *RTL1as*) in the placental samples of cases 1 and 2. (B) Relative mRNA expression levels for *DLK1*, *RTL1*, and *DIO3* against *GAPDH* (mean ± SE), in the equal amount of expression positive placental cells (vascular endothelial cells and pericytes) of cases 1 and 2 (corrected for the difference in the relative proportion of expression positive cells between the placental samples of cases 1 and 2 and the control placental samples, on the assumption that the *DLK1* expression level is "simply doubled" in the expression positive placental cells of case 1 and 2).

IHC examinations identified RTL1, DLK1 and DIO3 protein expressions in the vascular endothelial cells and pericytes of chorionic villi, but not in the cytotrophoblasts, syncytiotrophoblasts, and stromal cells, in the placentas of cases 1–3 and in the control placenta. The PEGs protein expression level was variable in the control placenta, with moderate DLK1 expression, high RTL1 expression, and low DIO3 expression. Furthermore, DLK1 protein expression was apparently stronger in the placentas of cases 1 and 2 than in the placenta of case 3 and the control placenta, RTL1 protein expression was obviously stronger in the placentas of cases 1–3 than in the control placenta, and DIO3 protein expression was apparently similar between the placentas of cases 1–3 and the control placenta.

Discussion

We studied placental samples obtained from cases 1–3 with typical body and placental upd(14)pat phenotype. In this regard, the microsatellite data suggest that upd(14)pat with heterodisomic and isodisomic loci in case 1 was caused by trisomy rescue or gamete complementation, and that upd(14)pat with isodisomic loci alone in case 2 resulted from monosomy rescue or postzygotic mitotic error, although it is possible that heterodisomic locus/loci remained undetected in case 2.[15] Notably, there was no trace of a maternally inherited locus indicative of the presence of trisomic cells or normal cells with biparentally inherited chromosome 14 homologs in the placentas as well as in the leukocytes of cases 1 and 2. In addition, the microdeletion of case 3 has been shown to be inherited from the mother with the same microdeletion.[2] These findings imply that the placental tissues as well as the leukocytes of cases 1–3 almost exclusively, if not totally, consisted of cells with upd(14)pat or those with the microdeletion.

The q-PCR analysis was performed for the fresh placental samples of cases 1 and 2. In this context, two matters should be pointed out. First, the proportion of vascular endothelial cells and pericytes expressing *DLK1*, *RTL1*, and *DIO3* would be somewhat variable among samples, because only a small portion of the placenta was analyzed. This would be relevant to the some degree of difference in the expression levels between the placental samples of cases 1 and 2. Second, the relative proportion of vascular endothelial cells and pericytes expressing *DLK1*, *RTL1*, and *DIO3* would be higher in the placental samples of cases 1 and 2 than in the control placental samples, because the placentas of cases 1 and 2 were accompanied by proliferation of the chorionic villi with such expression positive cells. Thus, it would be inappropriate to perform a simple comparison of relative expression levels against *GAPDH* between the placental samples of cases 1 and 2 and the control placental samples. Indeed, although a complex regulatory mechanism(s), as implicated for the *RTL1* expression,[1,2] is unlikely to be operating for the *DLK1* expression, the relative *DLK1* expression level was 3.3 times and 3.1 times, not 2 times, higher in the placental samples of cases 1 and 2 than in the control placental samples, respectively (**Fig. 3A**). Assuming that *DLK1* expression level is simply doubled in expression positive cells of cases 1 and 2, it is predicted that the relative proportion of such expression positive cells is 1.65 times (3.3 ÷ 2.0) and 1.55 times (3.1 ÷ 2.0) larger in the placental samples of cases 1 and 2 than in the control placental samples, respectively. Thus, the expression level against *GAPDH* in the equal

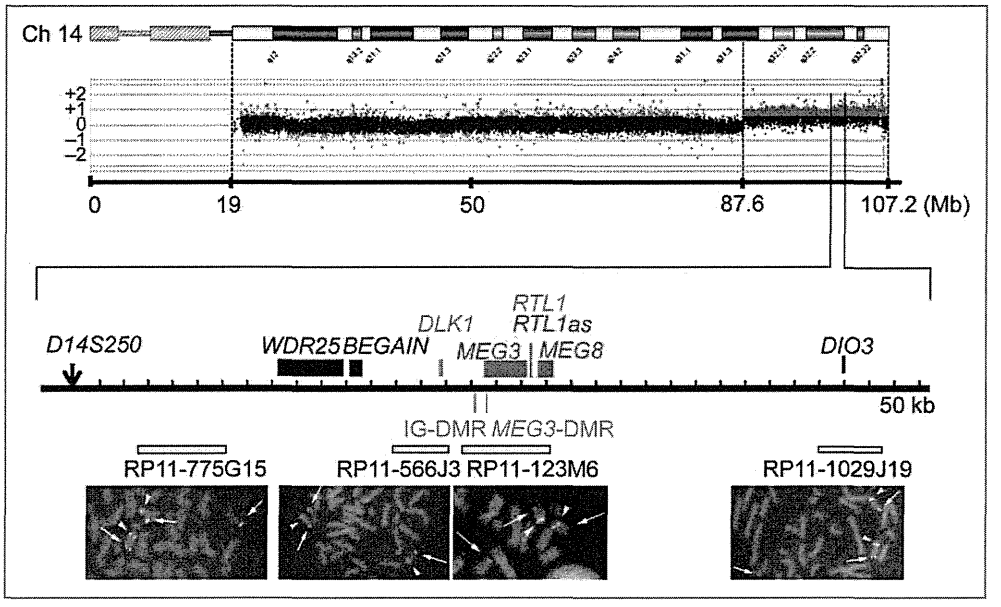

Figure 4. Array CGH and FISH analysis for the distal chromosome 14 region in case 4. In CGH analysis, the black, the red, and the green dots denote signals indicative of the normal, the increased (> +0.5), and the decreased (< −1.0) copy numbers, respectively. In FISH analysis, red signals (arrows) are derived from the probes detecting the various parts of the 14q32.2 imprinted region (the physical positions are indicated with yellow bars), and the green signals (arrowheads) are derived from an RP11−566I2 probe for 14q11.2 used as an internal control.

amount of expression positive cells is estimated as 3.69 times (6.1 ÷ 1.65) increased for *RTL1* and 1.15 times (1.9 ÷ 1.65) increased for *DIO3* in case 1, and as 6.06 times (9.4 ÷ 1.55) increased for *RTL1* and 1.09 times (1.7 ÷ 1.55) increased for *DIO3* in case 2 (**Fig. 3B**).

Thus, the expression data are summarized as follows (**Fig. 6**). First, it is inferred that the relative *RTL1* expression level is markedly (~5 times) increased in the expression positive cells of the placentas with upd(14)pat, as compared with the control placentas. This degree of elevation is grossly similar to that identified in the body of mice with the targeted deletion of the maternally derived IG-DMR (~4.5 times).[5] Such a markedly increased *RTL1* expression would be explained by assuming that *RTL1as*-encoded microRNAs (e.g., *miR433* and *miR127*) function as a repressor for *RTL1* expression through the RNAi mechanism, as has been indicated for the mouse *Rtl1-Rtl1as* interaction.[16,17] Second, it is unlikely that *DIO3* is solely expressed from the paternally inherited allele, although it remains to be determined whether *DIO3* undergoes partial imprinting like mouse *Dio3*[12] or completely escapes imprinting. In either case, the results would explain why patients with upd(14)pat and upd(14)mat lack clinically recognizable thyroid disorders,[2] although *DIO3* plays a critical role in the inactivation of thyroid hormones.[18]

This study provides further support for a critical role of excessive *RTL1* expression in the development of upd(14)pat phenotype (**Fig. 6**). Indeed, markedly (~5 times) increased *RTL1* expression is shared in common by cases 1–3 with typical upd(14)pat body and placental phenotype. In this context, it is notable that case 4 had no clinically recognizable upd(14)pat body and placental phenotype, except for omphalocele. This would imply that a single copy of *RTL1as* can almost reduce the *RTL1* expression dosage below the threshold level for the development of upd(14)pat phenotype by exerting a trans-acting repressor effect on the two functional copies of *RTL1*. By contrast, the relevance of *DLK1* to upd(14)pat phenotype is unlikely, because case 3 exhibited typical upd(14)pat phenotype in the presence of a single functional copy of *DLK1*, and case 4 showed no upd(14)pat phenotype except for omphalocele in the presence of two functional copies of *DLK1*. Similarly, if *DIO3* were more or less preferentially expressed from paternally inherited allele, the relevance of *DIO3* to upd(14)pat phenotype would also remain minor, if any. Case 4 had no upd(14)pat phenotype except for omphalocele in the presence of with two copies of *DIO3* of paternal origin. It should be pointed out, however, that the absence of *MEGs* expression may have a certain effect on the development of upd(14)pat phenotype.

The placental histological examinations revealed several informative findings. First, DLK1, RTL1, and DIO3 proteins were specifically identified in vascular endothelial cells and pericytes of chorionic villi in the control placenta, with RTL1 protein being most strongly expressed. These results, together with abnormal LM and EM findings of such cells in cases 1–3, suggest that these proteins, especially RTL1 protein, plays a pivotal role in the development of endothelial cells and pericytes. In this regard, it may be possible that the endothelial thickening and resultant narrowing the capillary lumens in the terminal villi have resulted in the dilatation of the stem to intermediate portions of the chorionic villi.

Second, the degree of protein staining was well correlated with the expression dosage of corresponding genes. In this regard, since characteristic macroscopic and microscopic placental features were identified in cases 1–3 who shared markedly elevated RTL1 protein expression, this is consistent with the notion that upd(14)pat phenotype is primarily caused by the markedly

elevated *RTL1* expression.[2] Indeed, DLK1 protein expression was not exaggerated in case 3 with typical upd(14)pat phenotype, and DIO3 protein expression was not enhanced in cases 1–3. It may be possible, however, that the abnormality of placental structures may have resulted in a difference in immunostaining without an actual change in gene expression. This point awaits further investigations.

Third, villous chorangiosis, stromal expansion, and mesenchymal dysplasia were not identified in the placental samples of cases 1–3, although such a lesion(s) may have existed in non-examined portions. Notably, such lesions are frequently observed in placentas of patients with BWS.[19-21] Thus, while both upd(14)pat and BWS are associated with placentomegaly and polyhydroamnios, characteristic histological findings appear to be different between upd(14)pat and BWS.

This study would also provide useful information on the methylation patterns of the *MEG3*-DMR in the placenta. Our previous studies using formalin-fixed and paraffin-embedded placental samples revealed that roughly two-thirds of clones were hypermethylated and the remaining roughly one-third of clones were hypomethylated in case 3 as well as in the previously reported patients with upd(14)pat (not cases 1 and 2) and epimutation (hypermethylation of the IG-DMR and the *MEG3*-DMR of maternal origin), and that roughly one-third of clones were hypermethylated and the remaining roughly two-thirds of clones were hypomethylated in control placental samples (see Fig. S2C in ref. 2). However, this study showed that the *MEG3*-DMR was grossly hypomethylated in the fresh placental samples of cases 1 and 2, with an extent similar to that identified in the fresh control placental samples. In this regard, it is notable that PCR products could be obtained only after 35 cycles for the formalin-fixed and paraffin-embedded placental samples and were sufficiently obtained after 30 cycles for the fresh placental samples. Thus, several specific clones may have been selectively amplified in the previous study. Furthermore, it may be possible that efficacy of bisulfite treatment (conversion of unmethylated cytosine into uracils and subsequently thymines) may be insufficient for the formalin-fixed and paraffin-embedded placental samples. Thus, it appears that the present data denote precise methylation patterns of the *MEG3*-DMR in the placenta.

In summary, the present study provides useful clues for the clarification of regulatory mechanism for the *RTL1* expression, imprinting status of *DIO3* and characteristic placental histological findings in patients with upd(14)pat and related conditions. Further studies will help improve our knowledge about upd(14)pat and related conditions.

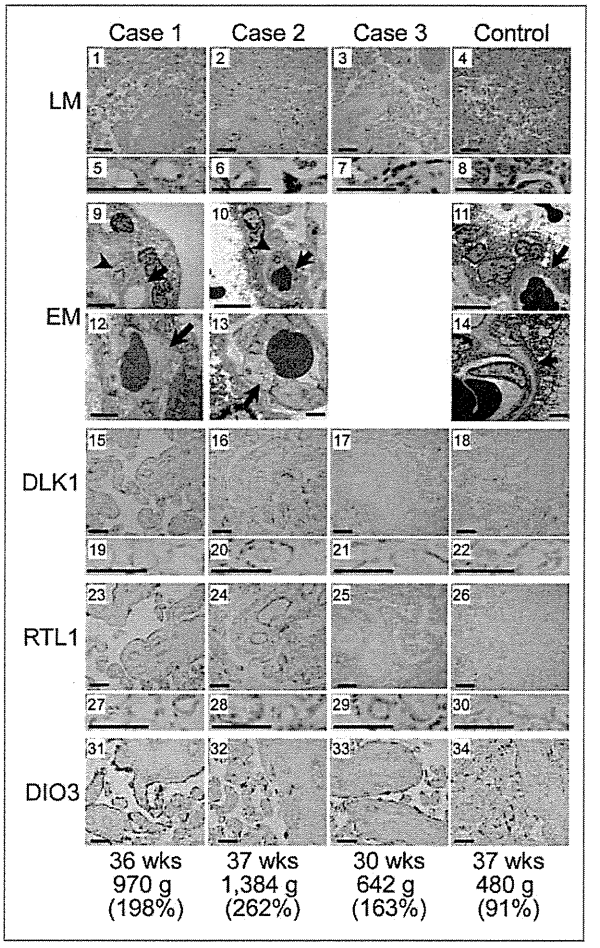

Figure 5. Histological examinations. LM, light microscopic examinations; EM, electron microscopic examinations; DLK1, RTL1 and DIO3, immunohistochemical examinations for the corresponding proteins. The arrows and arrowheads in the EM findings indicate endothelial cells and pericytes, respectively. Scale bars represent 100 μm for 1–4, 15–18, 23–26 and 31–34, 50 μm for 5–8, 19–22 and 27–30, 5 μm for 9–11 and 2 μm for 12–14. Gestational age, placental weight, and % placental weight assessed by the gestational age-matched Japanese references for placental weight[4,22] are described.

Methods

Ethical approval. This study was approved by the Institutional Review Board Committees of each investigator, and performed after obtaining written informed consent.

Primers. Primers utilized in this study are summarized in Table S3.

Sample preparation for molecular studies. Genomic DNA samples were obtained from leukocytes using FlexiGene DNA Kit (Qiagen) and from placental samples using ISOGEN (Nippon Gene). Transcripts of *DLK1, MEG3, RTL1, MEG8* and *DIO3* were isolated with ISOGEN (Nippon Gene), and *microRNAs* were extracted with mirVana™ miRNA Isolation Kit (Ambion). After DNase treatment, cDNA samples for *DLK1, MEG3, MEG8* and *DIO3* were prepared with oligo(dT) primers from 1 μg of RNA using Superscript III Reverse Transcriptase (Invitrogen), and those of *microRNAs* were synthesized from 300 ng of RNA using TaqMan MicroRNA Reverse Transcription Kit (Applied Biosystems). For *RTL1*, 3'-RACE was utilized to prevent amplification of *RTL1as*; cDNA was synthesized from 1 μg of RNA using Superscript III Reverse Transcriptase with a long primer hybridizing to poly A site and introducing the adaptor sequence. Lymphocyte metaphase spreads for FISH analysis were prepared from leukocytes using colcemide (Invitrogen).

Molecular studies. Microsatellite analysis for 19 loci on chromosome 14, methylation analysis for the IG-DMR and

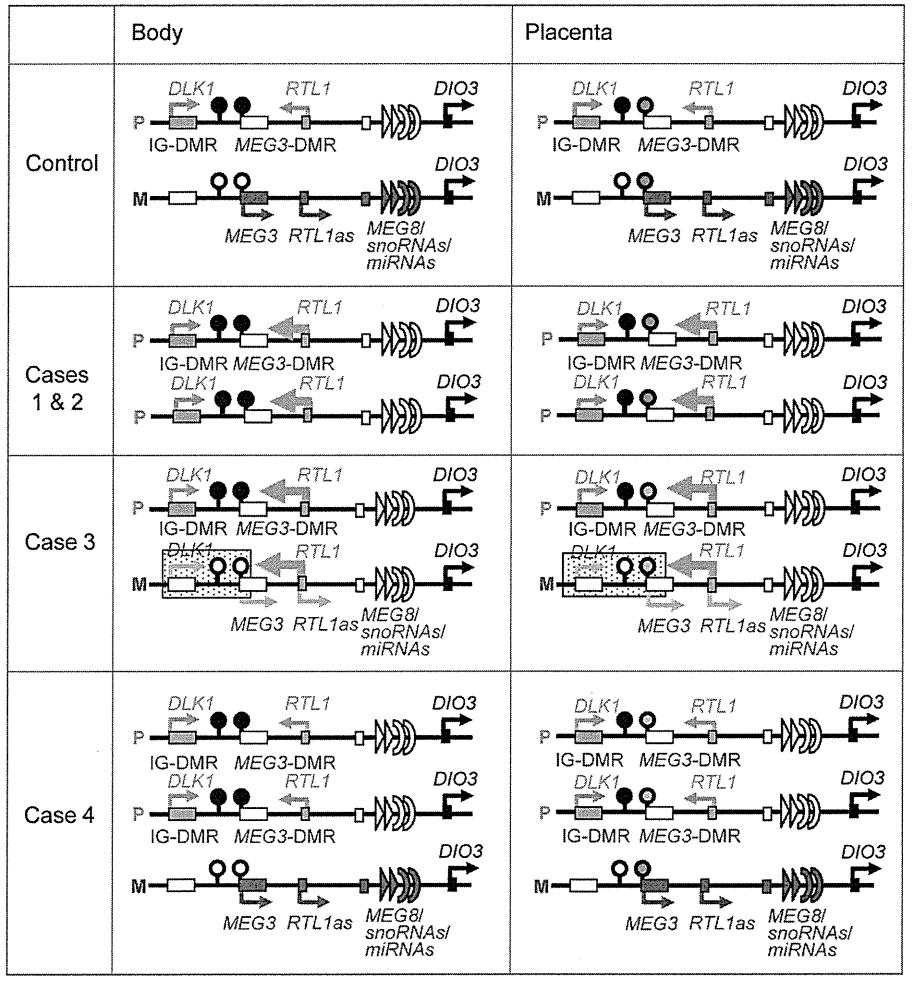

Figure 6. Schematic representation of the chromosome 14q32.2 imprinted region in a control subject, cases 1 and 2 with upd(14)pat, case 3 with a microdeletion (indicated by stippled rectangles), and case 4 with two copies of the imprinted region of paternal origin and a single copy of the imprinted region of maternal origin. This figure has been constructed using the present results and the previous data.[2,3] P, paternally derived chromosome; M, maternally derived chromosome. Filled and open circles represent hypermethylated and hypomethylated DMRs, respectively; since the *MEG3*-DMR is grossly hypomethylated and regarded as non-DMR in the placenta, it is painted in gray. *PEGs* (*DLK1* and *RTL1*) are shown in blue, *MEGs* (*MEG3*, *RTL1as*, *MEG8*, *snoRNAs* and *miRNAs*) in red, a probably non-imprinted gene (*DIO3*) in black, and non-expressed genes in white. Thick arrows for *RTL1* in cases 1–3 represent increased *RTL1* expression that is ascribed to loss of functional microRNA-containing *RTL1as* as a repressor for *RTL1*.

the *MEG3*-DMR, and FISH analyses for the 14q32.2 region were performed as described previously.[2,3] For FISH analysis of 17p13.3, a 17p sub-telomere probe and an RP11–411G7 probe for the 17p13.3 region were utilized, together with a CEP17 probe for the 17p11.1 region utilized as an internal control. The 17p sub-telomere probe was detected according to the manufacture's protocol, the RP11–411G7 probe was labeled with digoxigenin and detected by rhodamine anti-digoxigenin, and the CEP17 control probe was labeled with biotin and detected by avidin conjugated to fluorescein isothiocyanate. Quantitative real-time PCR analysis was performed on an ABI PRISM 7000 (Applied Biosystems) using TaqMan real-time PCR probe primer mixture for the following genes (assay No: Hs00171584 for *DLK1*, Hs00292028 for *MEG3*, Hs00419701 for *MEG8* and Hs00704811 for *DIO3*; assay ID: 001028 for *miR433* and 000452 for *miR127*). For *RTL1*, q-PCR analysis was performed with a forward primer hybridized to the sequence of *RTL1* and a reverse primer hybridized to the adaptor sequence. Fifty nanongrams of cDNA in a 50 μl reaction mixture contacting 2 × KOD FX buffer (Toyobo), 2.0 mM dNTP mixture (Toyobo), KOD FX (Toyobo), SYBR Green I (Invitrogen), and primer set for *RTL1* were subjected to the ABI PRISM 7000. Data were normalized against *GAPDH* (catalog No: 4326317E) for *DLK1*, *MEG3*, *MEG8*, *RTL1*, and *DIO3*, and against *RNU48* (assay ID: 0010006) for *microRNAs*. The expression studies were performed three times for each sample. Oligoarray CGH was performed using 1 × 1M format Human Genome Array (Catalog No G4447A) (Agilent Technologies).

Histopathological analysis. Placental samples were fixed with 20% buffered formaldehyde at room temperature and embedded in paraffin wax according to standard protocols for LM examinations. Then, sections of 3 μm thick were stained with hematoxylin-eosin. For EM examinations, fresh placental tissues were fixed with phosphate-buffered 2.5% glutaraldehyde, postfixed in 1% osmium tetroxide, and embedded in Epon 812 (catalog No. R3245, TAAB). Semithin sections were stained with 1% methylene blue, and ultrathin sections were double-stained with uranyl acetate and lead citrate. Subsequently, they were examined with a Ninhon Denshi JEM-1230 electron microscope.

For IHC analysis, sections of 3 μm thick were prepared by the same methods utilized for the LM examinations, and were examined with rabbit anti human DLK1 polyclonal antibody at 1:100 dilutions (catalog No 10636-1-AP, ProteinTech Group), rabbit anti human RTL1 polyclonal antibody at 1:200 dilutions, and rabbit anti human DIO3 polyclonal antibody at 1:50 dilutions (catalog No ab102926, abcam); anti human RTL1 polyclonal antibody was produced by immunizing rabbits with the synthesized RTL1 peptide (NH2-RGFPRDPSTESG-COOH) in this study. Sections were dewaxed in xylene and rehydrated through graded ethanol series and, subsequently, incubated in 10% citrate buffer (pH 6.0) for 40 min in a 98°C water bath, for antigen retrieval. Endogenous peroxidase activity was quenched with 1% H_2O_2 and 100% methanol for 20 min. To prevent non-specific background staining, sections are incubated with Protein Block Serum-Free (Dako corporation) for 10 min at room temperature. Then, sections were incubated overnight with primary antibody at 4°C

and, subsequently, treated with the labeled polymer prepared by combining amino acid polymers with peroxidase and anti- rabbit polyclonal antibody (Histofine Simple Stain MAX PO MULTI, Nichirei). Peroxidase activities were visualized by diaminobenzidine staining, and the nuclei were stained with hematoxylin.

Disclosure of Potential Conflicts of Interest

No potential conflicts of interest were disclosed.

Acknowledgments

This work was supported by Grants-in-Aid for Scientific Research (A) (22249010) and Research (B) (21028026) from the Japan Society for the Promotion of Science (JSPS), by Grants-in-Aid for Scientific Research on Innovative Areas (22132004-A04) from the Ministry of Education, Culture, Sports, Science and Technology (MEXT), by Grants for Research on Intractable Diseases (H22–161) from the Ministry of Health, Labor and Welfare (MHLW), by Grant for National Center for Child Health and Development (23A-1), and by Grant from Takeda Science Foundation and from Novartis Foundation.

Supplemental Materials

Supplemental materials may be found here:
www.landesbioscience.com/journals/epigenetics/article/21937

References

1. da Rocha ST, Edwards CA, Ito M, Ogata T, Ferguson-Smith AC. Genomic imprinting at the mammalian Dlk1-Dio3 domain. Trends Genet 2008; 24:306-16; PMID:18471925; http://dx.doi.org/10.1016/j.tig.2008.03.011.
2. Kagami M, Sekita Y, Nishimura G, Irie M, Kato F, Okada M, et al. Deletions and epimutations affecting the human 14q32.2 imprinted region in individuals with paternal and maternal upd(14)-like phenotypes. Nat Genet 2008; 40:237-42; PMID:18176563; http://dx.doi.org/10.1038/ng.2007.56.
3. Kagami M, O'Sullivan MJ, Green AJ, Watabe Y, Arisaka O, Masawa N, et al. The IG-DMR and the MEG3-DMR at human chromosome 14q32.2: hierarchical interaction and distinct functional properties as imprinting control centers. PLoS Genet 2010; 6:e1000992; PMID:20585555; http://dx.doi.org/10.1371/journal.pgen.1000992.
4. Kagami M, Yamazawa K, Matsubara K, Matsuo N, Ogata T. Placentomegaly in paternal uniparental disomy for human chromosome 14. Placenta 2008; 29:760-1; PMID:18619672; http://dx.doi.org/10.1016/j.placenta.2008.06.001.
5. Lin SP, Youngson N, Takada S, Seitz H, Reik W, Paulsen M, et al. Asymmetric regulation of imprinting on the maternal and paternal chromosomes at the Dlk1-Gtl2 imprinted cluster on mouse chromosome 12. Nat Genet 2003; 35:97-102; PMID:12937418; http://dx.doi.org/10.1038/ng1233.
6. Sekita Y, Wagatsuma H, Nakamura K, Ono R, Kagami M, Wakisaka N, et al. Role of retrotransposon-derived imprinted gene, Rtl1, in the feto-maternal interface of mouse placenta. Nat Genet 2008; 40:243-8; PMID:18176565; http://dx.doi.org/10.1038/ng.2007.51.
7. Lage JM. Placentomegaly with massive hydrops of placental stem villi, diploid DNA content, and fetal omphaloceles: possible association with Beckwith-Wiedemann syndrome. Hum Pathol 1991; 22:591-7; PMID:1864589; http://dx.doi.org/10.1016/0046-8177(91)90237-J.
8. Yamazawa K, Kagami M, Nagai T, Kondoh T, Onigata K, Maeyama K, et al. Molecular and clinical findings and their correlations in Silver-Russell syndrome: implications for a positive role of IGF2 in growth determination and differential imprinting regulation of the IGF2-H19 domain in bodies and placentas. J Mol Med (Berl) 2008; 86:1171-81; PMID:18607558; http://dx.doi.org/10.1007/s00109-008-0377-4.
9. Georgiades P, Watkins M, Burton GJ, Ferguson-Smith AC. Roles for genomic imprinting and the zygotic genome in placental development. Proc Natl Acad Sci U S A 2001; 98:4522-7; PMID:11274372; http://dx.doi.org/10.1073/pnas.081540898.
10. Fowden AL, Sibley C, Reik W, Constancia M. Imprinted genes, placental development and fetal growth. Horm Res 2006; 65(Suppl 3):50-8; PMID:16612114; http://dx.doi.org/10.1159/000091506.
11. Georgiades P, Ferguson-Smith AC, Burton GJ. Comparative developmental anatomy of the murine and human definitive placentae. Placenta 2002; 23:3-19; PMID:11869088; http://dx.doi.org/10.1053/plac.2001.0738.
12. Tsai CE, Lin SP, Ito M, Takagi N, Takada S, Ferguson-Smith AC. Genomic imprinting contributes to thyroid hormone metabolism in the mouse embryo. Curr Biol 2002; 12:1221-6; PMID:12176332; http://dx.doi.org/10.1016/S0960-9822(02)00951-X.
13. Yamanaka M, Ishikawa H, Saito K, Maruyama Y, Ozawa K, Shibasaki J, et al. Prenatal findings of paternal uniparental disomy 14: report of four patients. Am J Med Genet A 2010; 152A:789-91; PMID:20186803; http://dx.doi.org/10.1002/ajmg.a.33247.
14. Suzumori N, Ogata T, Mizutani E, Hattori Y, Matsubara K, Kagami M, et al. Prenatal findings of paternal uniparental disomy 14: Delineation of further patient. Am J Med Genet A 2010; 152A:3189-92; PMID:21108407; http://dx.doi.org/10.1002/ajmg.a.33719.
15. Kagami M, Kato F, Matsubara K, Sato T, Nishimura G, Ogata T. Relative frequency of underlying genetic causes for the development of UPD(14)pat-like phenotype. Eur J Hum Genet 2012; 20:928-32; PMID:22353941; http://dx.doi.org/10.1038/ejhg.2012.26.
16. Seitz H, Youngson N, Lin SP, Dalbert S, Paulsen M, Bachellerie JP, et al. Imprinted microRNA genes transcribed antisense to a reciprocally imprinted retrotransposon-like gene. Nat Genet 2003; 34:261-2; PMID:12796779; http://dx.doi.org/10.1038/ng1171.
17. Davis E, Caiment F, Tordoir X, Cavaillé J, Ferguson-Smith A, Cockett N, et al. RNAi-mediated allelic trans-interaction at the imprinted Rtl1/Peg11 locus. Curr Biol 2005; 15:743-9; PMID:15854907; http://dx.doi.org/10.1016/j.cub.2005.02.060.
18. Köhrle J. Thyroid hormone transporters in health and disease: advances in thyroid hormone deiodination. Best Pract Res Clin Endocrinol Metab 2007; 21:173-91; PMID:17574002; http://dx.doi.org/10.1016/j.beem.2007.04.001.
19. Kraus FT, Redline RW, Gersell DJ, Nelson DM, Dicker JM. Disorders of placental Development. Placental Pathology (Atlas of Noutumor Pathology). Washington, DC: American Registry of Pathology, 2004:59-68.
20. Fox HE, Sebire NJ. The placenta in abnormalities and disorders of the fetus. Pathology of the Placenta. Third edition, Philadelphia, PA: SAUNDERS, 2007:262-3.
21. Parveen Z, Tongson-Ignacio JE, Fraser CR, Killeen JL, Thompson KS. Placental mesenchymal dysplasia. Arch Pathol Lab Med 2007; 131:131-7; PMID:17227114.
22. Nakayama M. Placental pathology. Tokyo, Igaku Shoin, 2002:106-7 (in Japanese).

RESEARCH LETTER

AMERICAN JOURNAL OF medical genetics PART A

Recurrence of Osteogenesis Imperfecta Due to Maternal Mosaicism of a Novel *COL1A1* Mutation

Takahiro Yamada,[1]* Masaki Takagi,[2] Gen Nishimura,[3] Rina Akaishi,[1] Itsuko Furuta,[1] Mamoru Morikawa,[1] Takashi Yamada,[1] Kazutoshi Cho,[1] Hideaki Sawai,[4] Shiro Ikegawa,[5] Tomonobu Hasegawa,[2] and Hisanori Minakami[1]

[1]Department of Obstetrics and Gynecology, Hokkaido University Graduate School of Medicine, Sapporo, Japan

[2]Department of Pediatrics, Keio University School of Medicine, Tokyo, Japan

[3]Department of Radiology, Tokyo Metropolitan Children's Medical Center, Tokyo, Japan

[4]Department of Obstetrics and Gynecology, Hyogo College of Medicine, Nishinomiya, Japan

[5]Laboratory for Bone and Joint Diseases, Center for Genomic Medicine, RIKEN, Tokyo, Japan

Manuscript Received: 4 May 2012; Manuscript Accepted: 5 July 2012

TO THE EDITOR:

The lethal form of osteogenesis imperfecta (type II OI, OMIM #166210) is a common skeletal dysplasia that occurs during the perinatal period. Most cases are sporadic and attributable to heterozygous mutations of type 1 collagen genes (*COL1A1* and *COL1A2*). Therefore, type II OI is not likely to occur in siblings with normal parents; however, the occurrence of type II OI has been reported in 7–8% of siblings [Byers et al., 1988]. This is attributed in part to the autosomal recessive (AR) inheritance of OI because several genes encoding the enzymes involved in collagen post-translational modifications cause type II OI as AR traits [Barnes et al., 2006; Morello et al., 2006; Cabral et al., 2007; van Dijk et al., 2009; Lapunzina et al., 2010]. The occurrence of type II OI in siblings is also attributed to parental mosaics of type 1 collagen gene mutations [Byers et al., 1988; Cohen-Solal et al., 1991]. Indeed, several reports have described fatal outcomes from mosaic mutations in OI [Cohn et al., 1990; Constantinou et al., 1990; Wallis et al., 1990; Mottes et al., 1993; Cohen-Solal et al., 1994].

Here, we report on a family with recurrence of type II OI due to a *COL1A1* mosaic mutation in the mother. A 25-year-old Japanese woman reported a therapeutic abortion of her first pregnancy at 20 weeks of gestation due to shortening and bending of the long bones in her fetus. Neither tissue specimens nor radiographic images were obtained from the terminated fetus. She was referred to us at 17 weeks of gestation of her second pregnancy because bowing and shortening of the femora were found again in her second fetus. The mother was short in height (147 cm, −2.2 SD), but had no history of bone fracture and no clinical features of OI, such as blue sclera, hearing impairment, and abnormal tooth development. Her marriage was not consanguineous. Ultrasonography revealed a fetal biparietal diameter of 40.1 mm (+0.70 SD); lengths of the curved femur and humerus of 16.2 mm (−3.1 SD) and 14.2 mm (−3.8 SD), respectively; a narrowed thorax with short ribs; defective calvarial ossification evidenced by easy skull compression with an ultrasound probe (Fig. 1A); and unusually well-defined cerebral gyri.

How to Cite this Article:
Yamada T, Takagi M, Nishimura G, Akaishi R, Furuta I, Morikawa M, Yamada T, Cho K, Sawai H, Ikegawa S, Hasegawa T, Minakami H. 2012. Recurrence of osteogenesis imperfecta due to maternal mosaicism of a novel *COL1A1* mutation.
Am J Med Genet Part A 158A:2969–2971.

After genetic counseling with a tentative diagnosis of severe OI, the mother underwent a termination of the pregnancy at 19 weeks of gestation. Postmortem radiographs revealed beaded ribs, shortened broad and crumpled long bones, and nonossified calvaria, which warranted a diagnosis of type IIA OI (Fig. 1B). The parents did not permit an autopsy, but they gave consent for genetic examination of the umbilical cord blood and fetal skin sampled at the termination.

We extracted genomic DNA from the umbilical cord blood of the affected fetus and the peripheral blood of the unaffected parents by

Grant sponsor: Ministry of Health, Labour and Welfare of Japan; Grant numbers: H23-Nanchi-Ippan-123, H22-Nanchi-Ippan-194, Jitsuyoka (Nanbyo)-Ippan-014 (23300102).
Takahiro Yamada and Masaki Takagi contributed equally to this work.
*Correspondence to:
Takahiro Yamada, M.D., Ph.D., Department of Obstetrics and Gynecology, Hokkaido University Graduate School of Medicine, N15W7, Kita-ku, Sapporo 060-8638, Japan. E-mail: taka0197@med.hokudai.ac.jp
Article first published online in Wiley Online Library (wileyonlinelibrary.com): 17 September 2012
DOI 10.1002/ajmg.a.35602

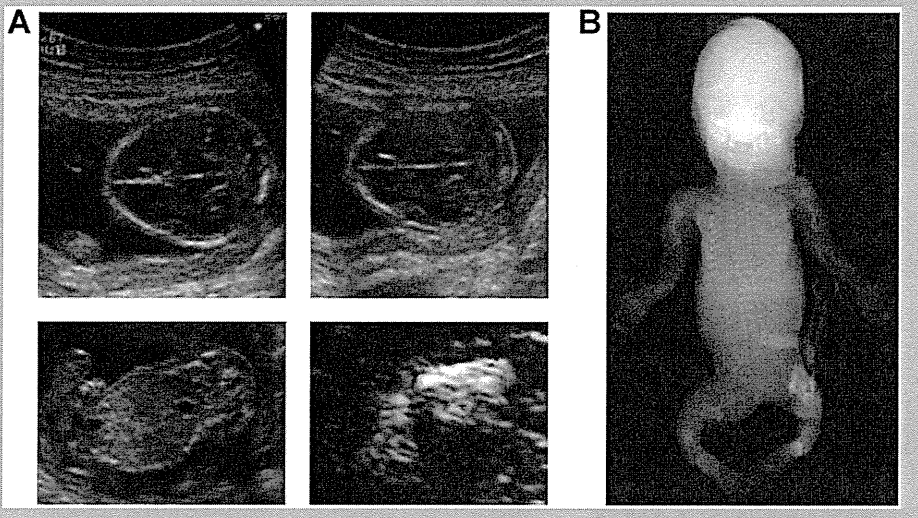

FIG. 1. A: Prenatal ultrasonography of the affected second fetus. Upper panels: Easily compressed unossified calvaria. The shape of the calvaria was easily changed before (left image) and after (right image) the compression. Lower left panel: Coronal view of the narrow thorax with short ribs. Lower right panel: Highly curved femur of the affected fetus. B: A postmortem radiograph of the fetus showing beaded ribs, shortened broad and crumpled long bones, and nonossified calvaria.

using a QIAamp DNA Mini Kit (Qiagen, Tokyo, Japan). We analyzed all coding exons and flanking introns of *COL1A1*, *COL1A2*, *LEPRE1*, *CRTAP*, and *PPIB* by polymerase chain reaction (PCR) of the genomic DNA and direct sequencing. A heterozygous mutation c.1054_1056 + 2 del AAGGT was found in *COL1A1* (Fig. 2A). Because the deletion involved the consensus splice donor site, a reverse transcription-PCR (RT-PCR) was performed using the fetus's RNA to check for a splicing abnormality. RNA was extracted from the fetal skin using an RNeasy Mini Kit (Qiagen). The cDNAs were subjected to PCR amplification using primers (5′-AAA TGG AGC TCC TGG TCA GA-3′ and 5′-AGG AGC ACC AGC AAT ACC AG-3′) encompassing exons 13–19. Sequencing of the RT-PCR products showed an insertion of 255 bp in intron 16, resulting in an in-frame insertion of 84 amino acids (Fig. 2B). *COL1A1* sequencing of the PCR products of the parents' genomic DNA from their blood samples revealed the same mutation in the mother, but not in the father. The electropherographic signal intensity of the mutant allele was low in the mother, suggesting a mosaic mutation (data not shown). The mosaic rate of this mutation was examined by subcloning of PCR products from genomic DNAs of various tissues; the ratio (mutant:wild-type) was 13:37 in blood, 16:34 in hair roots, and 8:42 in nails.

The mother became pregnant 3 months after the termination of her second pregnancy. A molecular examination of the chorionic villus sample excluded the *COL1A1* mutation (data not shown). She gave birth to an unaffected baby at 39 weeks of gestation. The mother underwent skeletal survey and dual energy X-ray absorptiometry for the lumbar spine (L2–L4) postpartum. Her bone mineral density was slightly low (0.865 g/cm^2; *Z*-score, −1.3), but still within the normal range. Radiographic examination revealed no abnormality suggestive of OI.

The unique *COL1A1* mutation reported here was predicted to cause mis-splicing and consequently to create an elongated procollagen protein. This elongated procollagen would presumably interfere the triple helix formation of collagen and hence is responsible for the lethal phenotypes of the affected siblings. This speculation is consistent with our current understanding of the pathogenesis of severe OI, which is believed to involve a dominant negative mechanism. As with the mother of fetus investigated in the current report, mosaic parents are sometimes asymptomatic or only mildly affected, if at all [Cohn et al., 1990; Constantinou et al., 1990; Wallis et al., 1990; Wijsman, 1991]. The mother showed only mildly short stature and mildly decreased bone density in the lumbar spine. The mosaic state of the mutation in the mother was 16–32% in the tissue examined. This observation was consistent with results of previous reports; a patient with 20% mosaic mutations in the blood and hair roots was asymptomatic [Cohn et al., 1990], while patients with 50% mutations in fibroblasts and 27% mutations in the blood were symptomatic [Wallis et al., 1990], and those with 25% mutations in fibroblasts and blood were also mildly symptomatic [Constantinou et al., 1990].

A molecular analysis to determine the mosaic state is important for familial recurrence. A genetic test, which confirms the mode of inheritance, followed by precise genetic counseling based on the recurrence rate estimation by mosaic rate, is particularly important in the management of severe perinatal OI.

ACKNOWLEDGMENTS

This study was supported by a Grant-in-Aid for Scientific Research from the Ministry of Health, Labour and Welfare of Japan, H23-Nanchi-Ippan-123 (to H.S., S.I.), H22-Nanchi-Ippan-194 (to T.H.) and Jitsuyoka (Nanbyo)-Ippan-014 (23300102) (to T.H.).

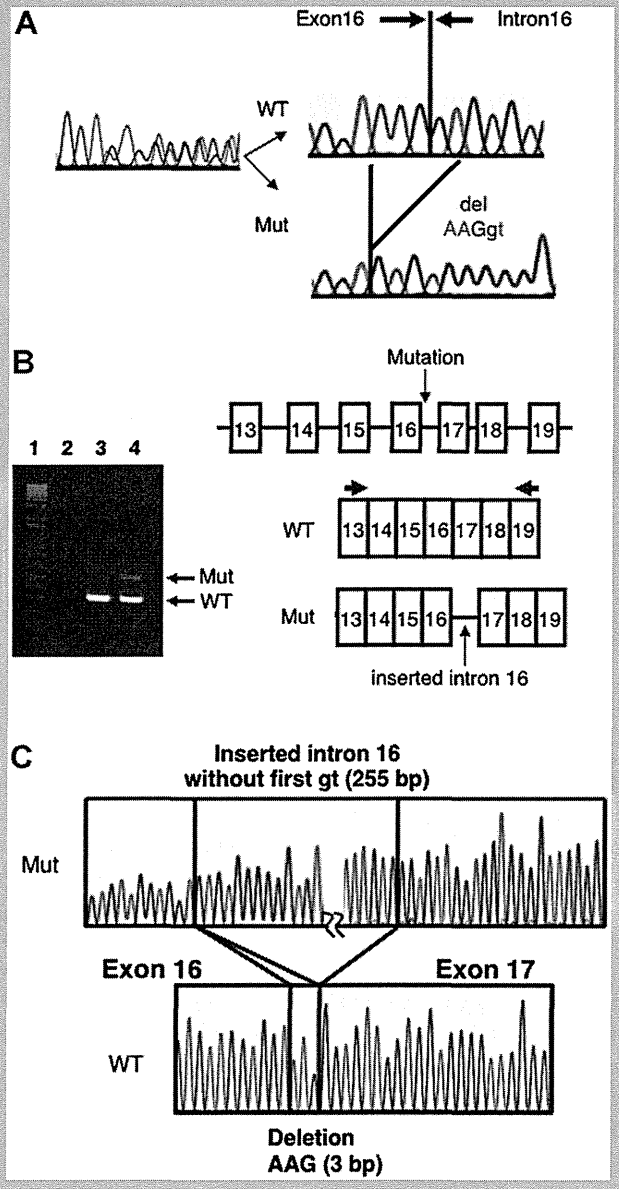

FIG. 2. ***COL1A1*** **mutation in the affected second fetus. A: Left: Direct sequencing of genomic DNA. The electropherograms of the wild-type (WT) and mutant (Mut) alleles were overlapping. Right: Subcloning revealed an AAGgt deletion in the junction of exon 16 and intron 16. B: RT-PCR of the mRNA from the fetal skin. Left: PCR products of WT (346 bp) and Mut (598 bp) are shown. Lanes 1: Marker, 2: Negative control, 3: Control cDNA, 4: Patient cDNA. Right: RT-PCR was performed using a primer set at exons 13 and 19 (arrows). C: cDNA sequence of the mutation. In the WT allele, intron 16 (257 bp) had been spliced out. The Mut allele had 5 bp deletion; "AAG" are the last 3 bp of exon 16 and "GT" are the first 2 bp of intron 16. The deletion of the splice donor site of intron 16 resulted in contiguous transcription to exon 16. The contiguous intron 16 was 255 bp long.**

REFERENCES

Barnes AM, Chang W, Morello R, Cabral WA, Weis M, Eyre DR, Leikin S, Makareeva E, Kuznetsova N, Uveges TE, Ashok A, Flor AW, Mulvihill JJ, Wilson PL, Sundaram UT, Lee B, Marini JC. 2006. Deficiency of cartilage-associated protein in recessive lethal osteogenesis imperfecta. N Engl J Med 355:2757–2764.

Byers PH, Tsipouras P, Bonadio JF, Starman BJ, Schwartz RC. 1988. Perinatal lethal osteogenesis imperfecta (OI type II): A biochemically heterogeneous disorder usually due to new mutations in the genes for type I collagen. Am J Hum Genet 42:237–428.

Cabral WA, Chang W, Barnes AM, Weis M, Scott MA, Leikin S, Makareeva E, Kuznetsova NV, Rosenbaum KN, Tifft CJ, Bulas DI, Kozma C, Smith PA, Eyre DR, Marini JC. 2007. Prolyl 3-hydroxylase 1 deficiency causes a recessive metabolic bone disorder resembling lethal/severe osteogenesis imperfecta. Nat Genet 39:359–365.

Cohen-Solal L, Bonaventure J, Maroteaux P. 1991. Dominant mutations in familial lethal and severe osteogenesis imperfecta. Hum Genet 87: 297–301.

Cohen-Solal L, Zylberberg L, Sangalli A, Gomez Lira M, Mottes M. 1994. Substitution of an aspartic acid for glycine 700 in the alpha 2(I) chain of type I collagen in a recurrent lethal type II osteogenesis imperfecta dramatically affects the mineralization of bone. J Biol Chem 269: 14751–14758.

Cohn DH, Starman BJ, Blumberg B, Byers PH. 1990. Recurrence of lethal osteogenesis imperfecta due to parental mosaicism for a dominant mutation in a human type I collagen gene (COL1A1). Am J Hum Genet 46:591–601.

Constantinou CD, Pack M, Young SB, Prockop DJ. 1990. Phenotypic heterogeneity in osteogenesis imperfecta: The mildly affected mother of a proband with a lethal variant has the same mutation substituting cysteine for alpha 1-glycine 904 in a type I procollagen gene (COL1A1). Am J Hum Genet 47:670–679.

Lapunzina P, Aglan M, Temtamy S, Caparrós-Martín JA, Valencia M, Letón R, Martínez-Glez V, Elhossini R, Amr K, Vilaboa N, Ruiz-Perez VL. 2010. Identification of a frameshift mutation in Osterix in a patient with recessive osteogenesis imperfecta. Am J Hum Genet 87:110–114.

Morello R, Bertin TK, Chen Y, Hicks J, Tonachini L, Monticone M, Castagnola P, Rauch F, Glorieux FH, Vranka J, Bächinger HP, Pace JM, Schwarze U, Byers PH, Weis M, Fernandes RJ, Eyre DR, Yao Z, Boyce BF, Lee B. 2006. CRTAP is required for prolyl 3- hydroxylation and mutations cause recessive osteogenesis imperfecta. Cell 127:291–304.

Mottes M, Gomez Lira MM, Valli M, Scarano G, Lonardo F, Forlino A, Cetta G, Pignatti PF. 1993. Paternal mosaicism for a COL1A1 dominant mutation (alpha 1 Ser-415) causes recurrent osteogenesis imperfecta. Hum Mutat 2:196–204.

van Dijk FS, Nesbitt IM, Zwikstra EH, Nikkels PG, Piersma SR, Fratantoni SA, Jimenez CR, Huizer M, Morsman AC, Cobben JM, van Roij MH, Elting MW, Verbeke JI, Wijnaendts LC, Shaw NJ, Högler W, McKeown C, Sistermans EA, Dalton A, Meijers-Heijboer H, Pals G. 2009. PPIB mutations cause severe osteogenesis imperfecta. Am J Hum Genet 85:521–527.

Wallis GA, Starman BJ, Zinn AB, Byers PH. 1990. Variable expression of osteogenesis imperfecta in a nuclear family is explained by somatic mosaicism for a lethal point mutation in the alpha 1(I) gene (COL1A1) of type I collagen in a parent. Am J Hum Genet 46:1034–1040.

Wijsman EM. 1991. Recurrence risk of a new dominant mutation in children of unaffected parents. Am J Hum Genet 48:654–661.

Novel Insights from Clinical Practice

Fetal Diagnosis and Therapy

Fetal Diagn Ther 2012;32:216–220
DOI: 10.1159/000335687

Received: July 13, 2011
Accepted after revision: December 7, 2011
Published online: February 18, 2012

A Case of Boomerang Dysplasia with a Novel Causative Mutation in Filamin B: Identification of Typical Imaging Findings on Ultrasonography and 3D-CT Imaging

Seiji Tsutsumi[a] Ayako Maekawa[a] Miyuki Obata[a] Timothy Morgan[b]
Stephen P. Robertson[b] Hirohisa Kurachi[a]

[a]Department of Obstetrics and Gynecology, Yamagata University Faculty of Medicine, Yamagata, Japan;
[b]Department of Paediatrics and Child Health, Dunedin School of Medicine, University of Otago, Dunedin, New Zealand

Established Facts

- Boomerang dysplasia is a rare lethal osteochondrodysplasia characterized by disorganized mineralization of the skeleton, leading to complete nonossification of some limb bones and vertebral elements and a boomerang-like aspect to some of the long tubular bones.

Novel Insights

- Demonstration of the characteristic bent bone morphology in the limbs by 3D-CT adds diagnostic certainty and facilitates prognostication and genetic counseling for parents.
- The mutation observed in this patient, c.605T>C, is the third causative mutation described in this disorder and, like the other two mutations, leads to substitution of an amino acid residue in the actin-binding domain of filamin B.

Key Words
Boomerang dysplasia · Fetal imaging · Filamin B

Abstract
Boomerang dysplasia is a rare lethal osteochondrodysplasia characterized by disorganized mineralization of the skeleton, leading to complete nonossification of some limb bones and vertebral elements, and a boomerang-like aspect to some of the long tubular bones. Like many short-limbed skeletal dysplasias with accompanying thoracic hypoplasia, the potential lethality of the phenotype can be difficult to ascertain prenatally. We report a case of boomerang dysplasia prenatally diagnosed by use of ultrasonography and 3D-CT imaging, and identified a novel mutation in the gene encoding the cytoskeletal protein filamin B *(FLNB)* postmortem. Findings that aided the radiological diagnosis of this condition in utero included absent ossification of two out of three long bones in each limb and elements of the vertebrae and a boomerang-like shape to the ulnae. The identified mutation is the third described for this disorder and is predicted to lead to amino acid substitution in the actin-binding domain of the filamin B molecule.

KARGER
Fax +41 61 306 12 34
E-Mail karger@karger.ch
www.karger.com

1015–3837/12/0323–0216$38.00/0

Accessible online at:
www.karger.com/fdt

Seiji Tsutsumi
Department of Obstetrics and Gynecology
Yamagata University Faculty of Medicine
2-2-2 Iida-Nishi, Yamagata 990-9585 (Japan)
Tel. +81 23 628 5393, E-Mail stsutsumi@med.id.yamagata-u.ac.jp

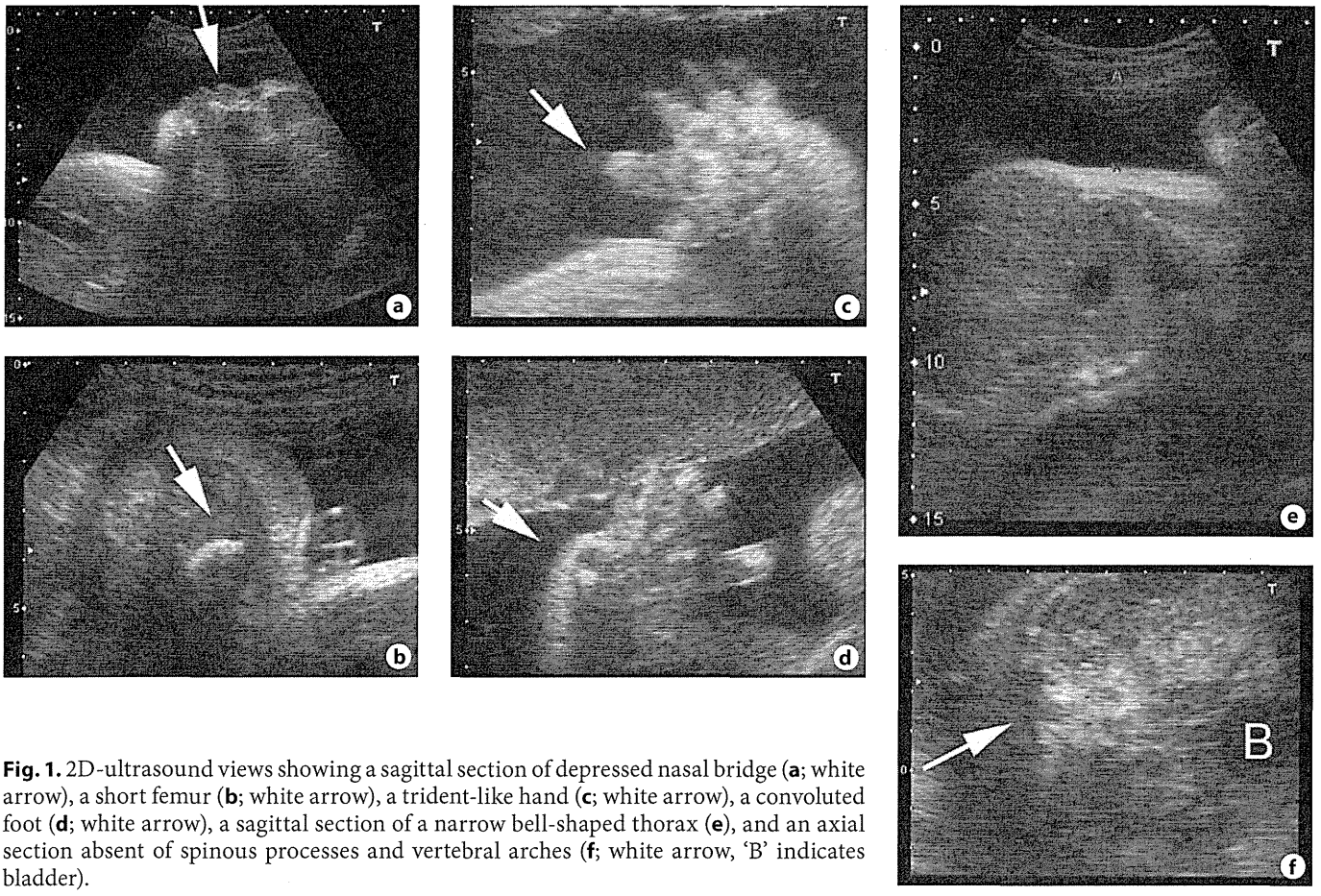

Fig. 1. 2D-ultrasound views showing a sagittal section of depressed nasal bridge (**a**; white arrow), a short femur (**b**; white arrow), a trident-like hand (**c**; white arrow), a convoluted foot (**d**; white arrow), a sagittal section of a narrow bell-shaped thorax (**e**), and an axial section absent of spinous processes and vertebral arches (**f**; white arrow, 'B' indicates bladder).

Clinical Report

This was the second pregnancy of unrelated healthy parents. The family history is noncontributory. At the time of conception the mother was 30 years old and the father 29. Routine ultrasound investigation in the 33rd week of gestation revealed severe fetal malformations, leading to referral to our hospital for prenatal diagnosis. Sonographic evaluation showed a fetus with severe micromelia. At the 33rd week of gestation, the fetal biparietal diameter was 84.8 mm (–0.3 SD), fetal trunk area was 5,808 mm^2 (–1.0 SD) and femur length was 18.2 mm (–14.8 SD). Only one of the three tubular bones was present in each limb, and the elbows and knees were indiscernible. The hands were trident and ossifications of the metacarpal bones were diminished. The bridge of the nose was flattened. The thorax was hypoplastic and had a bell-shaped appearance. The spinous processes and vertebral arches were not ossified (fig. 1). 3D-CT imaging showed the boomerang-like-shaped ulna, and the segment-shaped femur (fig. 2). In view of the typical skeletal abnormalities, including micromelia, and the absence of ossification of some but not all of the long tubular bones, the tentative diagnosis of boomerang dysplasia was made. After genetic counseling, the parents preferred not to resuscitate postpartum in view of the severity of the phenotype.

The fetus was born in the 38th week of gestation, and soon died from respiratory insufficiency. The bridge of the nose was defective (fig. 3) and a cleft palate was recognized. X-ray imaging confirmed the findings as demonstrated on the prenatal 3D-CT. Mutation analysis of the filamin B *(FLNB)* gene was undertaken on DNA extracted from umbilical cord blood after informed consent was obtained from the parents. All exons and exon-intron boundaries of *FLNB* were amplified using polymerase chain reaction as described previously [1], and amplified DNA was subjected to denaturing high-performance liquid chromatography with amplicons exhibiting anomalous waveforms subsequently sequenced on an ABI3100 sequencer. A novel mutation, c.605T>C, in exon 3 was identified, which is predicted to lead to the substitution of p.Met202Thr of the FLNB protein. This substitution occurs in the calponin homology 2 region of the actin-binding domain of FLNB.

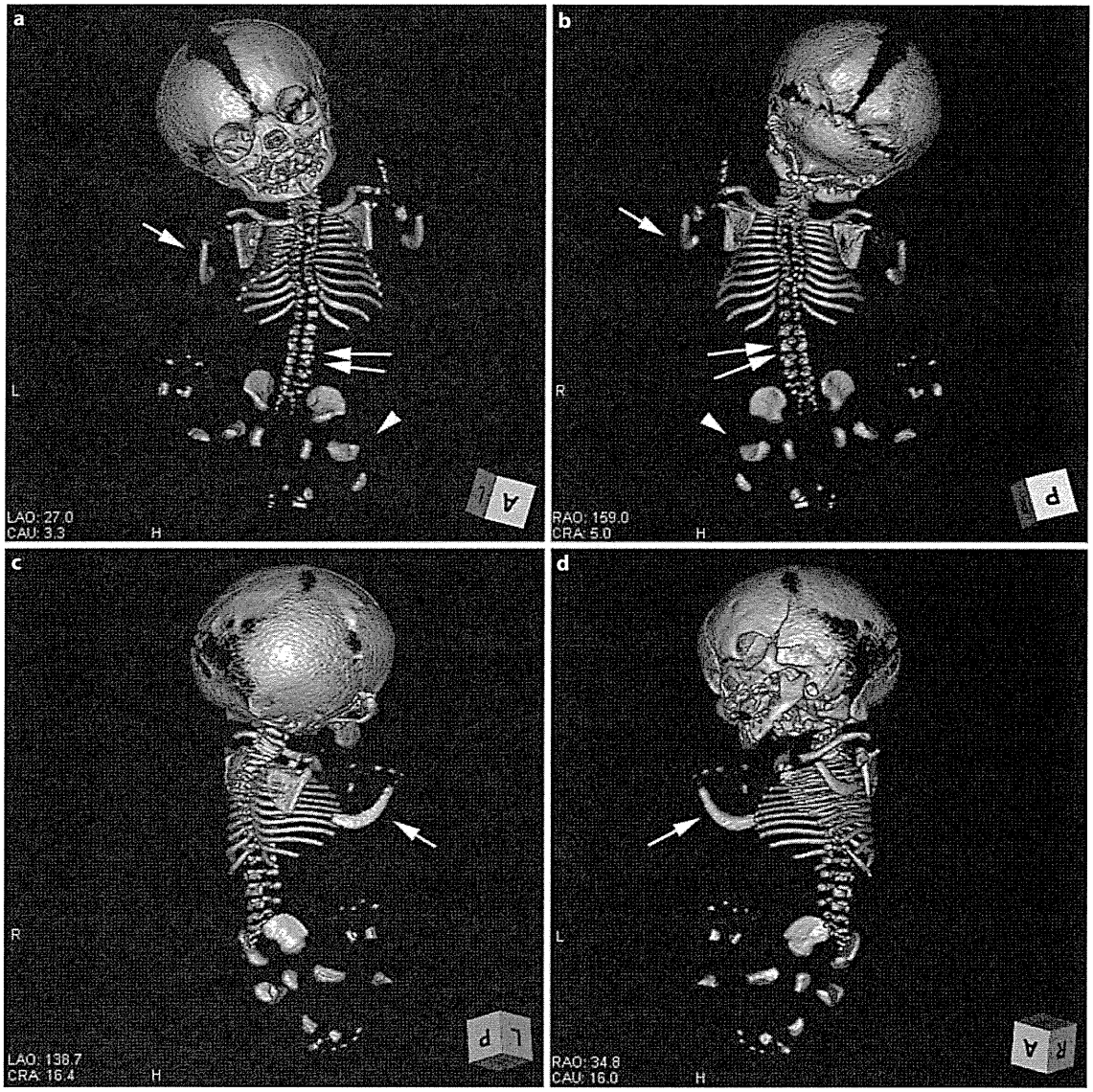

Fig. 2. 3D-CT views showing the boomerang-like shaped ulna (white arrow), the segment shaped femur (white arrow head) and zipper-like shaped spine (double arrows). The humerus and radius were absent: front view (**a**), rear view (**b**), right side view (**c**) and left side view (**d**).

Discussion

Boomerang dysplasia is a rare osteochondrodysplasia characterized by a boomerang-like aspect of the long tubular bones [2, 3]. It belongs to a family of skeletal dysplasias of varying severity, all caused by mutations in the same gene, *FLNB* [4, 5]. These related conditions in order of diminishing severity include atelosteogenesis type I and III [4] and Larsen syndrome [6]. Boomerang dysplasia is difficult to diagnose prenatally. All cases of this condition described in the literature thus far have been characterized by lethality, although instances of the phenotypically similar allelic condition, atelosteogenesis III, have been reported in conjunction with survivorship [7]. In this report we show that helical 3D-CT is a useful adjunct to obtain specific images of the skeletal abnormalities manifest in this condition.

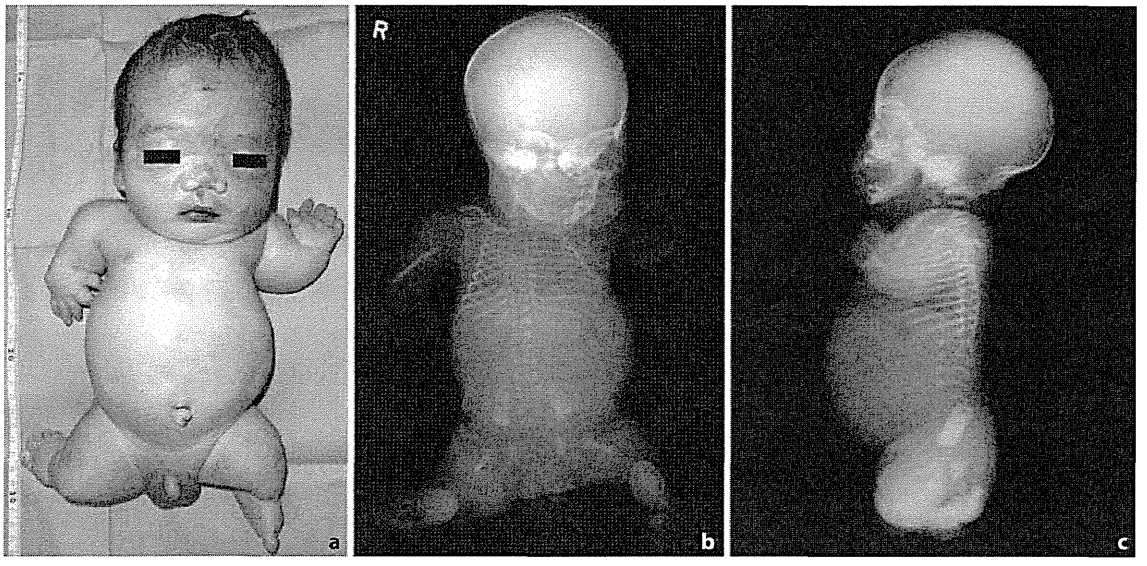

Fig. 3. The postmortem images of the patient. The nasal bridge was flattened, and the extremities were short and flexed: macroscopic front view (**a**), X-ray front view (**b**) and X-ray rear side view (**c**).

The key findings that facilitated the diagnosis of boomerang dysplasia in this instance included the absence of two of the three long bones in each limb, underossification of some components of the vertebrae and disordered ossification of the metacarpals. These findings can also be observed in atelosteogenesis type I, an observation that reflects the close phenotypic relatedness of these two conditions. Importantly, however, the milder potentially survivable condition, atelosteogenesis III, does not feature nonossification of the long bones of the limbs [4, 7]. In this instance demonstration of the characteristic bent bone morphology in the limbs by 3D-CT added diagnostic certainty and facilitated prognostication and genetic counseling for the parents. This was possible because the images obtained by 3D-CT enabled the visualization of some additional details of the fetal skeleton which were not clearly recognized in the ultrasonographic evaluation. Furthermore, the reconstructed 3D-CT enabled visualization of the whole fetal skeleton without contamination from maternal anatomy [8, 9].

The mutation observed in this patient, c.605T>C is the third causative mutation described in this disorder, and like the other two known mutations (p.Leu171Arg, p.Ser235Pro) leads to substitution of an amino acid residue in the actin-binding domain of FLNB [5]. Reflecting their close relatedness, a previously reported mutation, c.604A>G, occurring at the same codon predicts the substitution p.Met202Val and results in an atelosteogenesis I phenotype. The parents of our patient did not give permission to perform their own genetic analysis to check whether the change is de novo. However, this substitution (p.Met202Thr) changes polarity and hydrophilic property of the amino acid residue. Therefore, it might be pathogenic due to the potential of protein structural and functional change. Similar mutations leading to atelosteogenesis I and Larsen syndrome leads to an increased avidity of FLNB for cytoskeletal actin [10], but the mechanism by which this impacts on skeletogenesis and ossification of bone is not understood.

Acknowledgement

This article is supported by a Grant-in-Aid for Scientific Research from the Ministry of Health, Labour and Welfare of Japan (H23-Nanchi-Ippan-123).